Consensus Standards for Acquisition, Measurement, and Reporting of Intravascular OCT (IVOCT) Studies

A Report from The International Working Group for Intravascular OCT Standardization and Validation

Online Supplementary Material

The information described in this Online Supplementary Material augments the print version of the IVOCT consensus document (JACC Vol. 59, No. 12).

. This online material includes supplemental information on:

1) Levels of evidence bibliography for image interpretation
2) Equipment for IVOCT imaging
3) IVOCT artifacts
4) IVOCT image display techniques
5) Image acquisition protocols
6) Qualitative assessment
7) Quantitative measurement
8) IVOCT validation
9) Specialized OCT techniques
10) Reporting of IVOCT studies

A number of appendices to the consensus document are also provided here:

A. Technical glossary
B. Figure credits
C. Names and affiliations of the Writing Committee (WC)
D. Disclosure of financial interests for the WC

1. Levels of Evidence for IVOCT Image Interpretation Bibliography

As of the writing of this document, over 600 peer-reviewed manuscripts have been written on the topic of vascular OCT. Different groups have published more than 20 papers describing the correlation between OCT images and histology of normal and atherosclerotic blood vessels (1-25), providing much of the basis for image interpretation Levels of Evidence. Other papers that were considered by the IWG-IVOCT included clinical correlations with IVOCT features. In Online Table 1, we list different IVOCT image features, Levels of Evidence, and some representative accompanying references.

2. Equipment for IVOCT imaging

Catheters for IVOCT Examination

IVOCT catheters scan a focused beam of light circumferentially around the vessel and longitudinally along the vessel using mechanical systems. An IVOCT catheter contains a rotating *single-mode optical fiber* that is terminated at its distal end by a lens that focuses the beam and a reflector element, to direct it sideways to the vessel wall(107). The catheter is connected to a *rotary junction* that utilizes a motor unit to rotate the optical fiber in the catheter. The rotary junction also couples light from the stationary

optical fiber, from the IVOCT system console, to the rotating optical fiber in the catheter. The rotary junction is mounted on a translation stage or sled for motorized, automated pullback. Rotation and translation of the fiber in the catheter, actuated by the rotary junction and pullback motor units, is transmitted to the distal imaging tip by the optical fiber itself, or by a flexible drive cable encapsulating the fiber. For most IVOCT catheters, the drive cable, fiber, and optics are encapsulated in a transparent imaging sheath. For TD-OCT, the currently available imaging probe (ImageWire™ St. Jude Medical/LightLab Imaging Inc., Westford, MA, USA) has a maximum outer diameter of 0.019″ (with a standard 0.014" radiopaque coiled tip) and contains a single-mode fiber optic core within a translucent sheath. For FD-OCT, the imaging probes are integrated in a short monorail catheter (profile varies currently from 2.4 Fr to 3.2 Fr) compatible with conventional 0.014” angioplasty guide wires and 6 Fr or larger guiding catheters.

IVOCT Consoles and Controls

The console of the IVOCT system provides NIR light to, and collects light backscattered from, the vessel wall through the catheter and rotary junction. Within the console, the reflected light signals are detected and converted to digital signals, which are used to generate IVOCT images. The console additionally displays and archives IVOCT images.

The console may also be used to control the rotational and pullback speed of the catheter. Rotational speed determines both the rate at which individual circular cross-sectional images are obtained and in conjunction with the *A-line rate* of the IVOCT system, the number of A-lines per image. Similarly, the pullback speed determines the *pitch* of the *helical scan* or *frame-to-frame spacing* and therefore the spatial resolution along the *longitudinal dimension* of an L-mode IVOCT image.

The optical signal registered by the IVOCT console is mapped to a display value using either a pseudo-color or grayscale lookup table (Online Fig. 1). Console settings for the *gain* and dynamic range are used to determine this mapping and therefore control the quality of the displayed image. Controlling the gain causes the IVOCT signal to be amplified, which can be useful for improving the visualization of structures deep within the artery wall. However, gain values that are too high may saturate areas of higher *backscattering*, potentially making these regions difficult to interpret. Changing the dynamic range alters the range of minimum-to-maximum OCT signal values that are mapped into the range of gray scale values. A dynamic range that is too narrow will not display a sufficient number of gray scale values to accurately represent the image, resulting in an image that has high noise and less information content.

The Z-offset is an additional control that the console provides in order to ensure the fidelity of the spatial representation of the image that is required to make accurate measurements. Z-offset refers to slight variations in the *optical path length* of the optical fiber within the catheter*,* which manifests as incorrect image diameters and axial spatial calibration. Calibration can be accomplished by adjusting the optical path length in the sample and/or reference arm, which can be performed automatically, semi-automatically, or manually before each IVOCT examination. Also, the fiber length can change during a single pullback, resulting in a varying Z-offset across the IVOCT dataset. It is recommended that images be evaluated to ensure that the Z-offset is correct, and adjusted if necessary, before analysis.

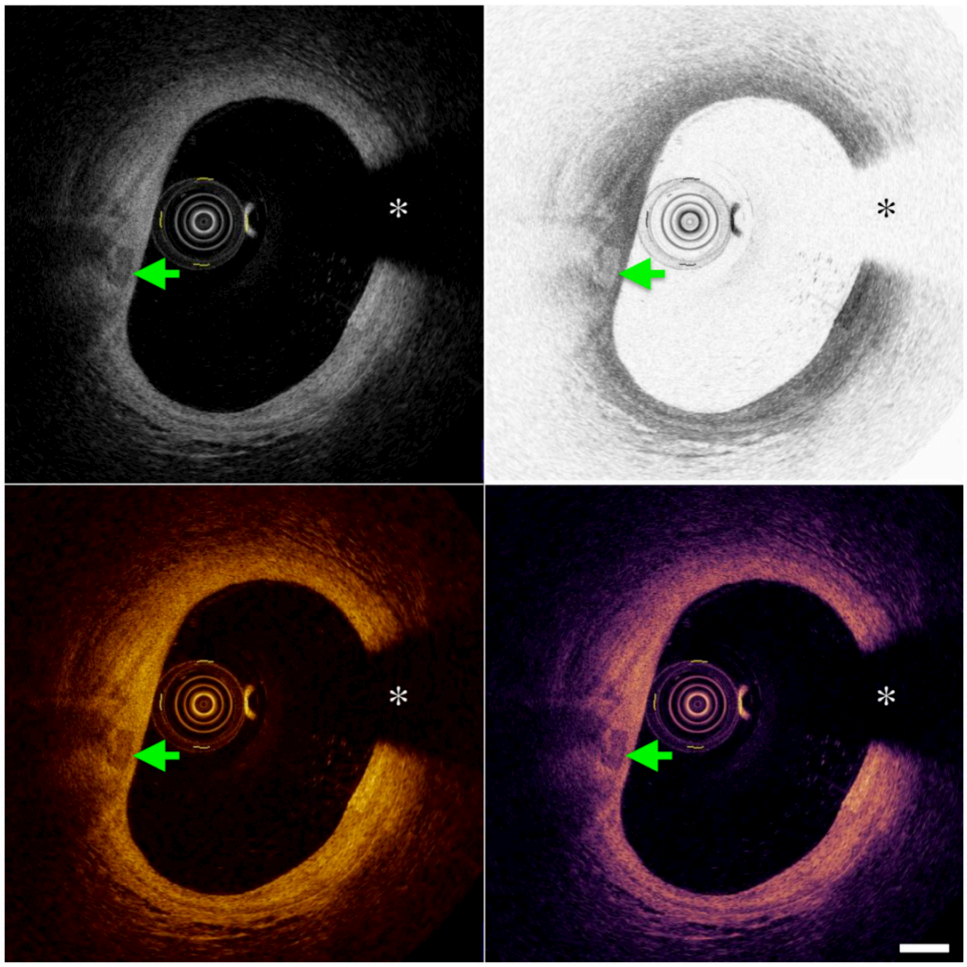

Online Figure 1. IVOCT images displayed using different look up tables (left upper – gray scale; right upper – inverse gray scale; left lower – sepia; right lower – thallium). Green arrow points to a focal calcific nodule that can be visualized in all of the images. * denotes guide wire artifact. Scale bar represents 500 μm. IVOCT technology, image contributor and institution, and commercial IVOCT vendor for each Figure is provided in Online Appendix B.

IVOCT DICOM Standard

A standard for storing and transferring digital IVOCT images and information is critical to ensure interoperability between different IVOCT imaging systems and *PACS* (Picture Archive and Communication System). DICOM (Digital Imaging and Communication in Medicine) is a standard for exchanging medical images and other information, between medical imaging devices.

Support for IVOCT is present in DICOM Supplement 151. Supplement 151 passed letter ballot in June of 2011 and is now part of the DICOM standard. Supplement 151 contains the Information Object Definitions required to document a DICOM IVOCT image. It introduces two new *service-object pair* (SOP) classes for IVOCT imaging. One SOP Class is used FOR PRESENTATION, the other used FOR PROCESSING. FOR PROCESSING IVOCT images are stored in *polar coordinates*, and contain all the information needed for conversion to Cartesian coordinate images. FOR PRESENTATION IVOCT images are *scan converted* with the appropriate corrections

applied for accurate measurements and display. The acquired images are monochrome. Since IVOCT images resemble IVUS images, a tint or pseudo-color look-up table is sometimes applied to differentiate IVOCT from IVUS. The Supplemental Palette *Color Lookup Table* (LUT) is used to convey tint information. Different pseudo-color presentation information may be applied through the use of a Palette LUT at a viewing station.

3. IVOCT Artifacts

Non-Uniform Rotational Distortion (NURD)

Non-uniform rotational distortion (NURD) is a consequence of mechanical catheter systems that arises from binding of the drive cable or rotating optical components during image acquisition. The artifact, also seen by mechanical IVUS systems with rotating transducers (108), appears as a smearing of the IVOCT signal in the rotational or circumferential direction (Online Fig. 2). This artifact can occur because of a defective catheter or increased friction on the rotating components. For example this artifact can be caused by tortuous vasculature; a constriction of the imaging sheath, including a tight hemostatic valve; a crimped imaging sheath; or passage of the catheter through a narrow stenosis.

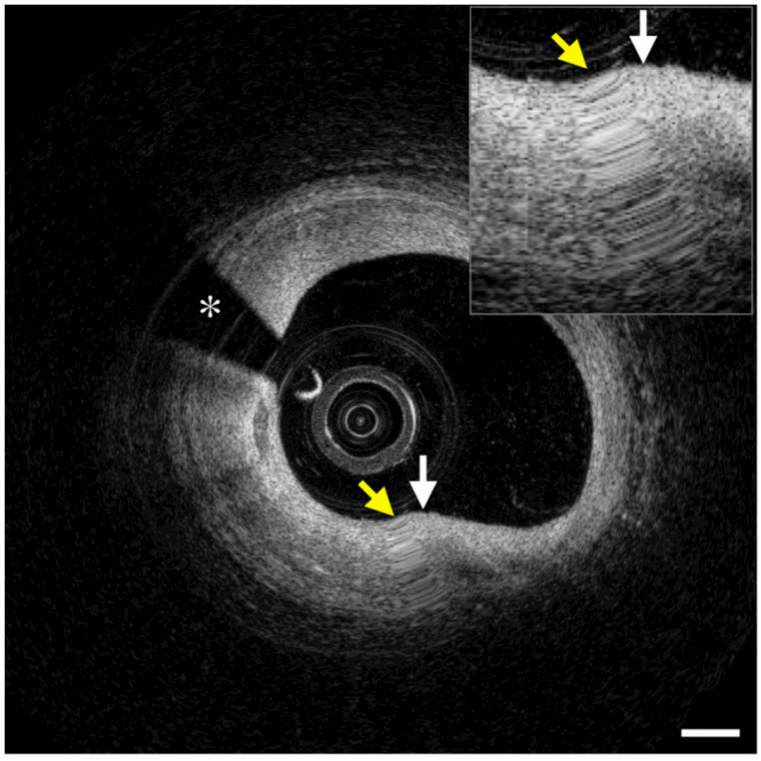

Online Figure 2. Non-uniform Rotational Distortion (NURD). Yellow arrow points to area that is smeared along the circumferential direction (inset, 2x), which results in a distortion of the lumen contour (white arrow). Scale bar represents 500 μm. IVOCT technology, image contributor and institution, and commercial IVOCT vendor for each Figure is provided in Online Appendix B. Abbreviations as in Online Figure 1.

Multiple reflections

For some catheters that have reflecting surfaces, the reflections may bounce off of multiple facets of the catheter, creating one or more circular lines within the image (Online Fig. 3). These artifacts should be identified and not interpreted as real tissue structure.

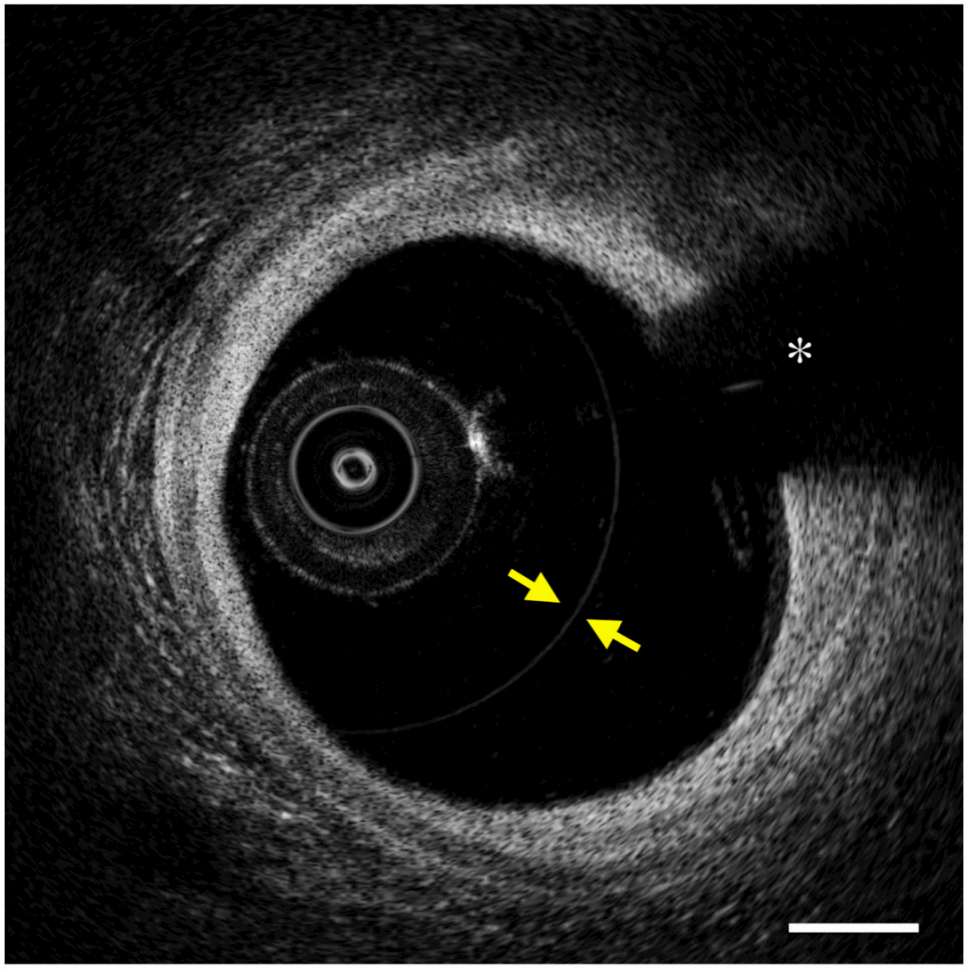

Online Figure 3. Multiple reflections. Arrows delineate a circular line that is likely caused by multiple reflections from the catheter. Scale bar represents 500 μm. IVOCT technology, image contributor and institution, and commercial IVOCT vendor for each Figure is provided in Online Appendix B. Abbreviations as in Online Figure 1.

Blooming

A blooming artifact occurs in IVOCT images where excess intensity, commonly seen at stent strut surfaces, creates the appearance of a bright reflector that is enlarged and smeared along the axial direction (Print Fig. 9B, green inset).

Saturation

When a high reflector is encountered by IVOCT light, it may be backscattered at too high an intensity to be accurately detected by the *detector*, thereby causing artifacts in the affected A-lines (Online Fig. 4). Structures that exhibit high backscattering commonly include the guide wire, the tissue surface, and metallic stent struts. *Saturation* artifacts appear as linear streaks of high and low intensities within the image along the axial direction.

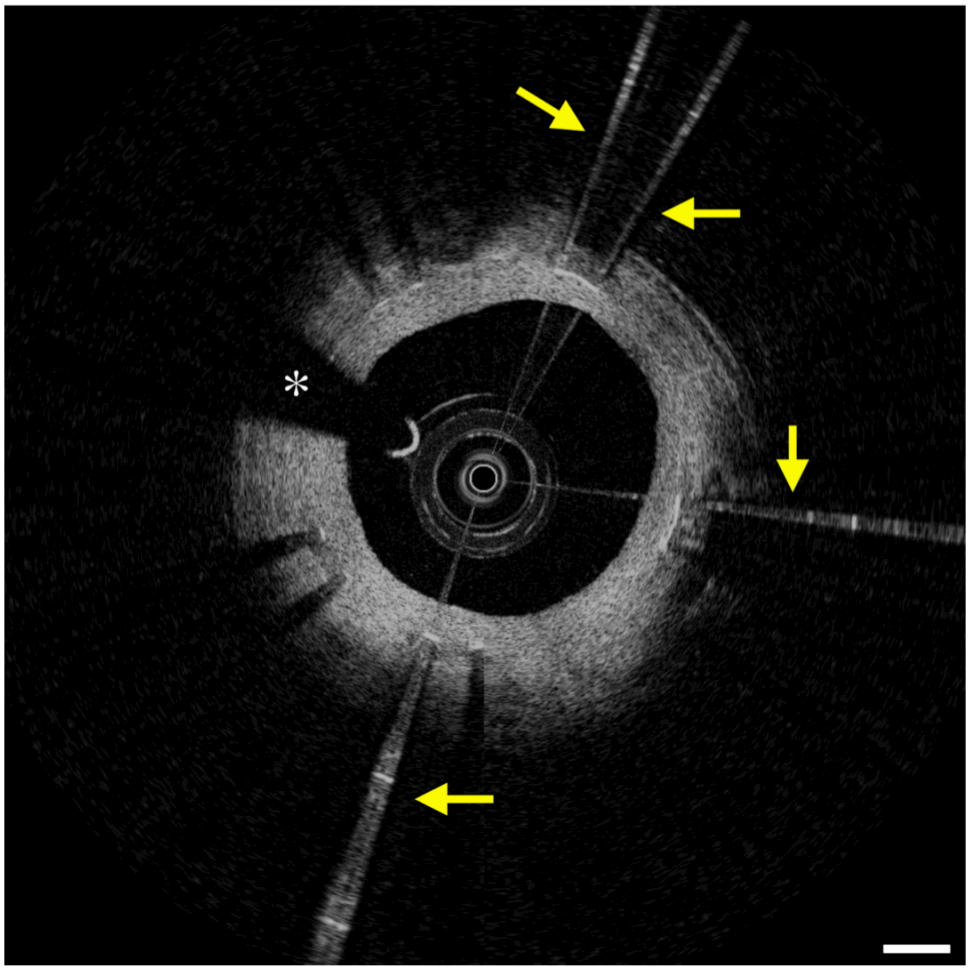

Online Figure 4. Saturation. Arrows point to high signal intensity artifacts that extend along the *axial dimension*. Scale bar represents 500 μm. IVOCT technology, image contributor and institution, and commercial IVOCT vendor for each Figure is provided in Online Appendix B. Abbreviations as in Online Figure 1.

Motion

Motion of the artery with respect to the catheter occurs in several dimensions and can cause multiple types of artifacts, affecting the cross-sectional and/or L-mode images. Changes in vessel dimensions during cardiac cycle can be observed. Typically, the lumen area is larger in end-diastole as compared to systole. If the catheter has moved with respect to the vessel during the time of a single cross-sectional image acquisition, an axial discontinuity termed a seam line (Online Fig. 5), may appear at the location of the transition between the first and the last A-line. This is best observed in cross-sectional image reconstructions. Longitudinal motion can result in disruption of the continuity of the pullback and results in the repeated appearances of similar anatomic features within the pullback. Motion artifacts also affect L-mode images, giving rise to oscillations that coincide with the cardiac cycle. Of note, FD-OCT systems have fewer motion artifacts caused by cardiac motion during the heart cycle than TD-OCT systems, as the pullback speed of FD-OCT is higher, enabling complete pullback imaging within a small number of cardiac cycles. The high pullback speed of FD-OCT systems may make it difficult to gate the images to the cardiac cycle post-hoc, however.

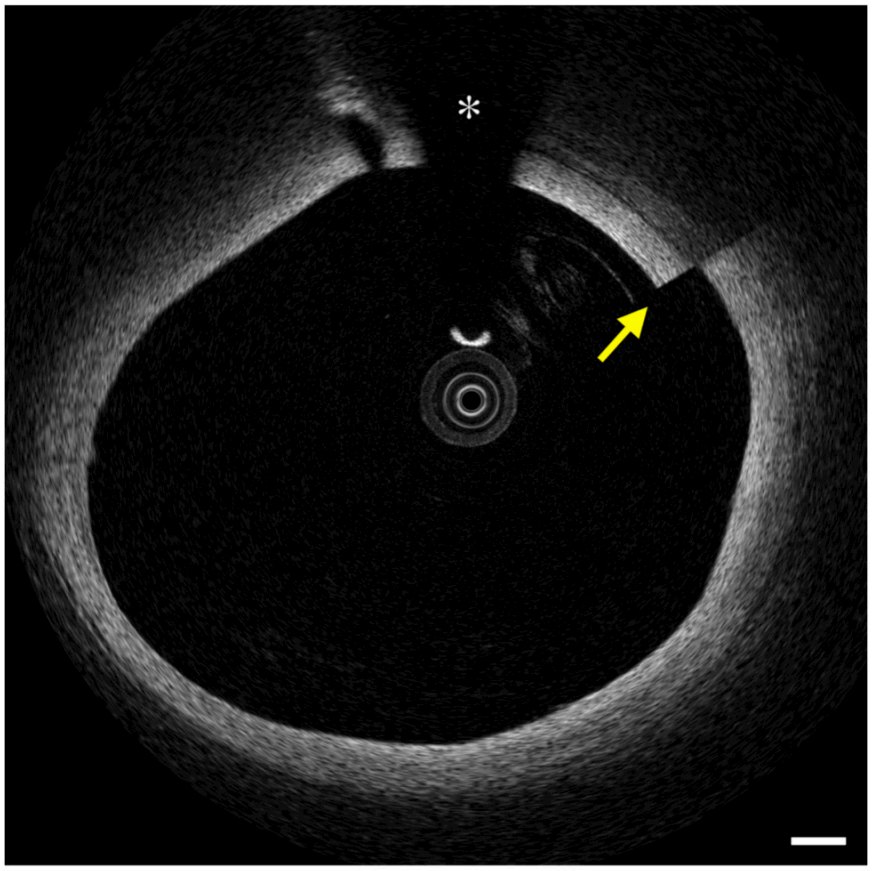

Online Figure 5. Seam Line. Arrow points to an apparent discontinuity in luminal surface that is caused by artery motion that occurs during the time between the first and last A-line of a cross-sectional image. Scale bar represents 500 μm. IVOCT technology, image contributor and institution, and commercial IVOCT vendor for each Figure is provided in Online Appendix B. Abbreviations as in Online Figure 1.

Foldover artifact

In FD-OCT systems, when the vessel is larger than the ranging depth, a portion of the vessel may appear to fold over in the image (Online Fig. 6). These portions of the image data that contain foldover artifact should not be interpreted.

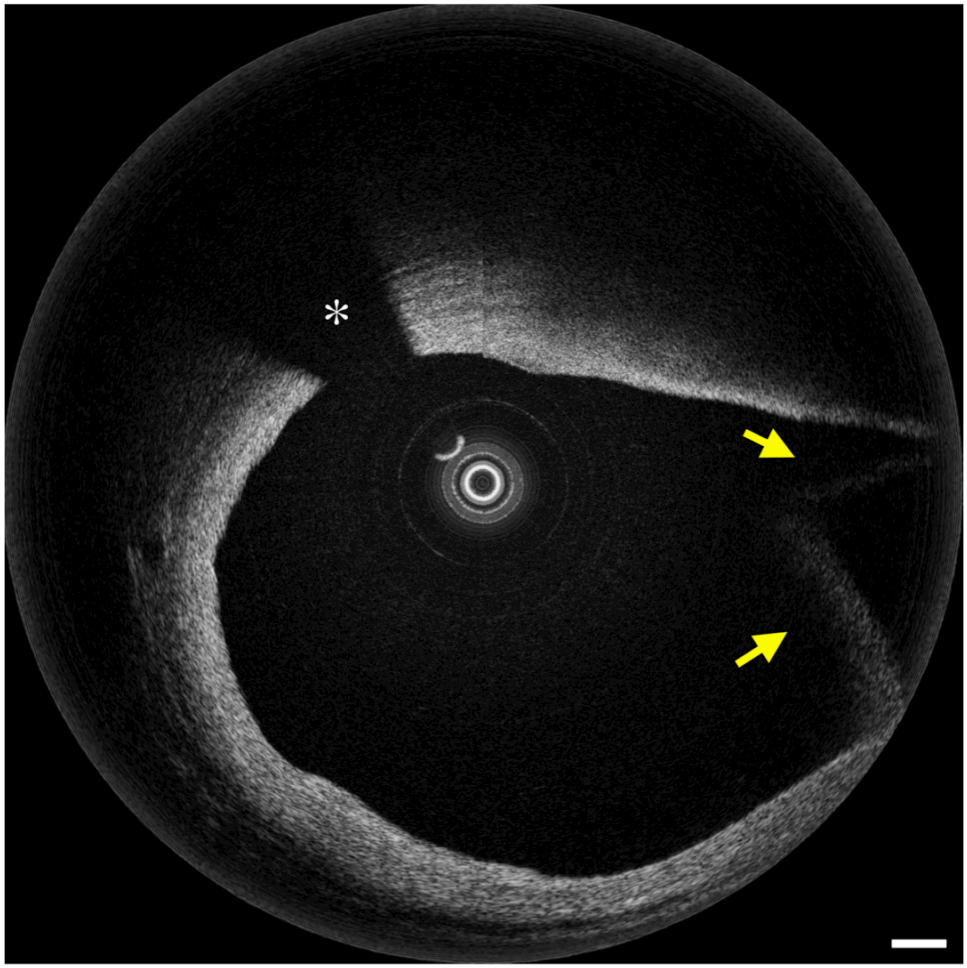

Online Figure 6. Foldover artifact. IVOCT image of a large vessel showing regions where the artery appears to fold over onto itself (arrows). Scale bar represents 500 μm. IVOCT technology, image contributor and institution, and commercial IVOCT vendor for each Figure is provided in Online Appendix B. Abbreviations as in Online Figure 1.

Speckle

Speckle is grainy noise that appears on IVOCT images that is a consequence of the way in which the image is formed. It is important to recognize the presence of speckle, which has a size scale on the order of the spatial resolution, so as to not interpret it as structure within the tissue.

Shadowing

A variety of objects can create shadows that appear as drops in signal intensity on the abluminal side of the objects in the IVOCT image. Shadows can completely occlude or may diminish the image intensity of deeper structures (Online Figs. 7-9). Common objects that create shadows in the IVOCT images are opaque, such as the guide wire and metallic stent struts. Air bubbles or defects in the sheaths of some catheters or blood in the catheter may also cause shadows. Blood in the catheter (Online Fig. 7) or the lumen (Online Fig. 8), or thrombus (Online Fig. 9) may create shadows in the image, making it difficult to visualize the underlying sector of artery wall. Macrophage accumulations may also create shadows in the image, potentially causing a plaque to appear as if it is a necrotic core.

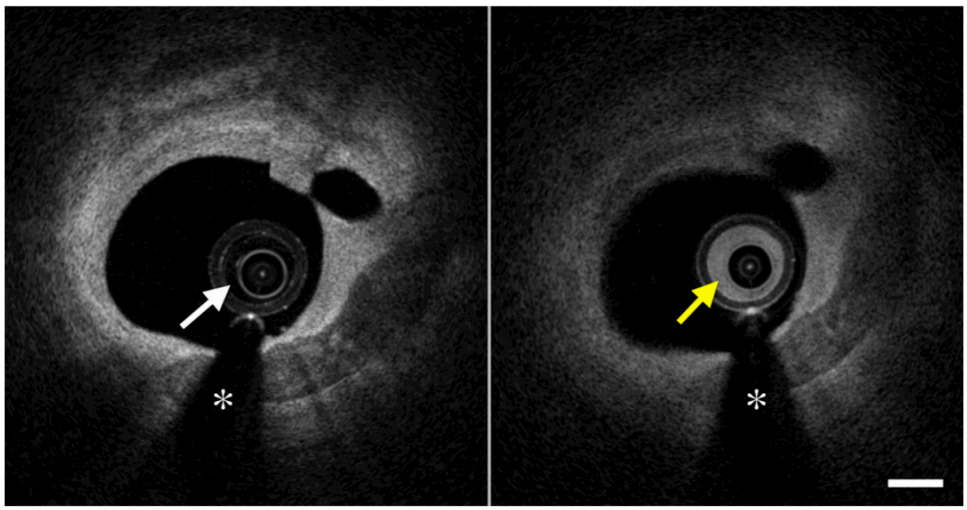

Online Figure 7. Shadowing caused by blood inside of catheter. Left panel shows low IVOCT signal within the catheter (white arrow) and good visualization of the artery wall. Right panel shows a high IVOCT signal from within the catheter (yellow arrow) and a relatively low IVOCT signal and blurred image features from the artery wall. Scale bar represents 500 μm. IVOCT technology, image contributor and institution, and commercial IVOCT vendor for each Figure is provided in Online Appendix B. Abbreviations as in Online Figure 1.

Suboptimal vessel flushing

When blood is inadequately cleared from the field of the view, the lumen can have a high IVOCT intensity (Online Fig. 8, upper left panel). Sometimes, when suboptimal vessel flushing occurs, the IVOCT image of the artery wall is of sufficient quality to allow interpretation (Online Fig. 8, upper left panel). In other cases, suboptimal vessel flushing diminishes the signal from the artery, resulting in unacceptable image quality (Online Fig. 8, lower left panel). Care should be taken when interpreting image data when blood within the lumen significantly affects the quality of the IVOCT image data from the artery wall.

Scattering and focus artifacts

Scattering or imaging away from the focus diminishes the IVOCT image intensity and decreases lateral resolution. For this reason, objects such as stent struts that are far from the focus or that are imaged through blood (Online Fig. 8, lower left panel) or other tissue may appear dimmer and/or larger than expected.

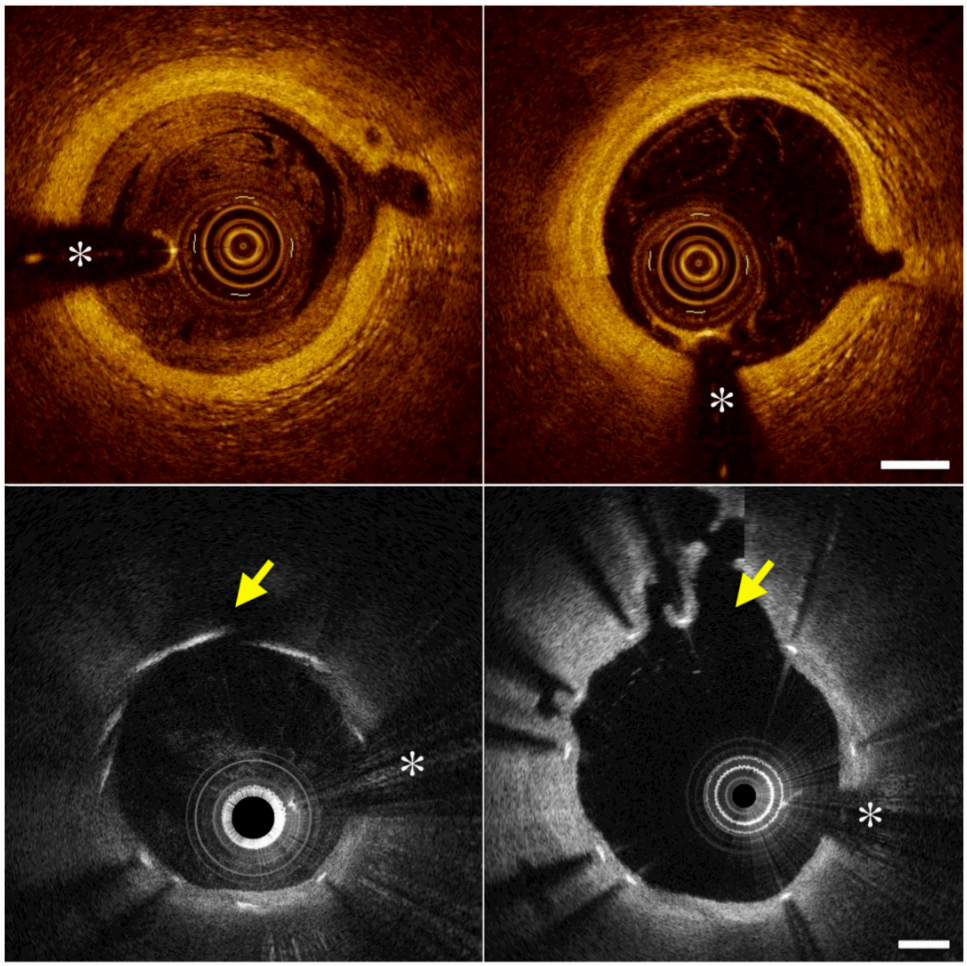

Online Figure 8. Suboptimal flushing. Top row – suboptimal flushing with acceptable image quality. Suboptimal flushing (upper left) with high signal intensity within the lumen, compared with improved but not perfect flushing (upper right) from the same location in the coronary artery. Bottom row – suboptimal flushing with unacceptable image quality. Suboptimal flushing (lower left) demonstrating decreased resolution, as evidenced by blurring and enlargement of stent struts, and lower image intensity, compared with improved flushing (lower right) from the same location in the coronary artery. The yellow arrow points to a side branch. Scale bars represent 500 μm. IVOCT technology, image contributor and institution, and commercial IVOCT vendor for each Figure is provided in Online Appendix B. Abbreviations as in Online Figure 1.

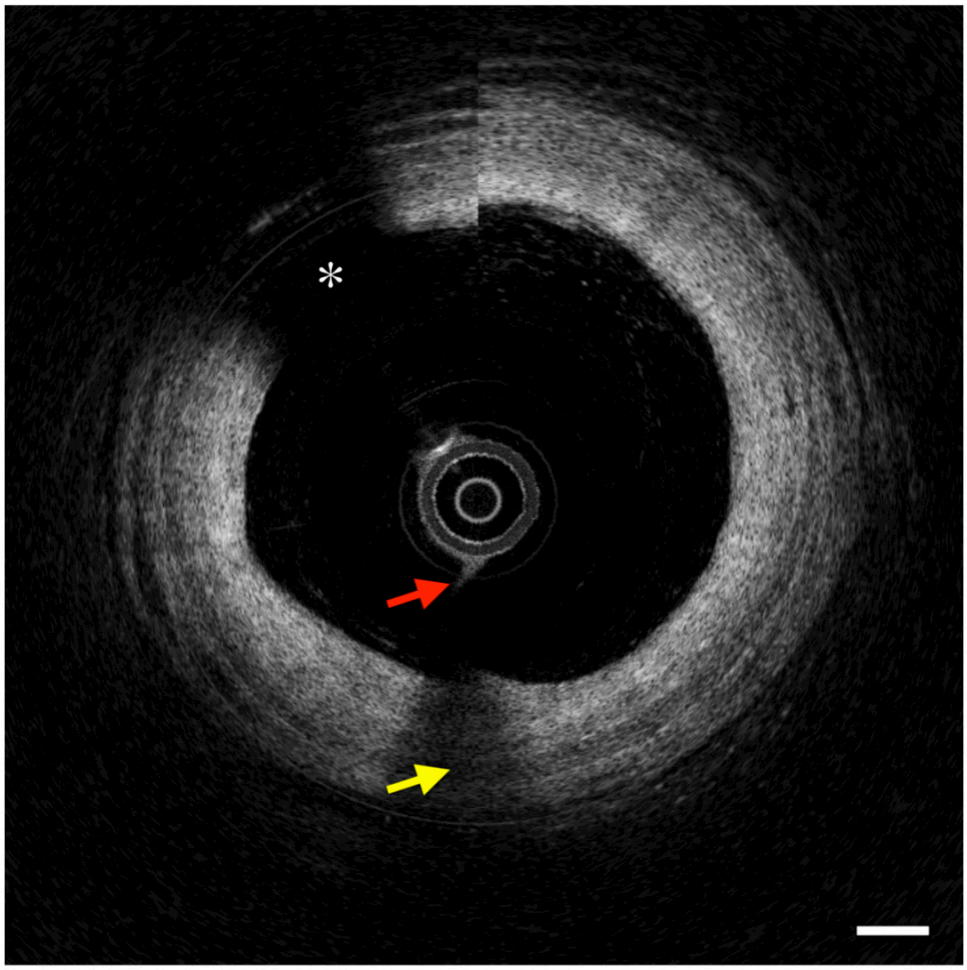

Online Figure 9. Shadowing. Tissue adherent to the catheter (red arrow), likely a small thrombus, attenuates the IVOCT signal at greater depths (yellow arrow). Scale bar represents 500 μm. IVOCT technology, image contributor and institution, and commercial IVOCT vendor for each Figure is provided in Online Appendix B. Abbreviations as in Online Figure 1.

Proximity artifact

Occasionally when the catheter is very near to or touching the artery wall, the IVOCT image gray scale values may be higher when the tissue is closer to the catheter. The physical mechanism that causes this phenomenon is presently unknown.

Tangential signal dropout

When the catheter is located near the vessel wall, the optical beam can be directed nearly parallel to the tissue surface. This artifact is more likely to occur when the catheter is against the artery and the vessel wall is flat or is raised adjacent to the catheter. In these situations, the light beam is attenuated as it passes along the surface of the artery wall and the resultant artery wall may appear signal poor below the luminal surface (Online Fig. 10, arrows). Whenever the catheter is situated in this manner, one should consider this artifact before evaluating the pathology of the artery wall.

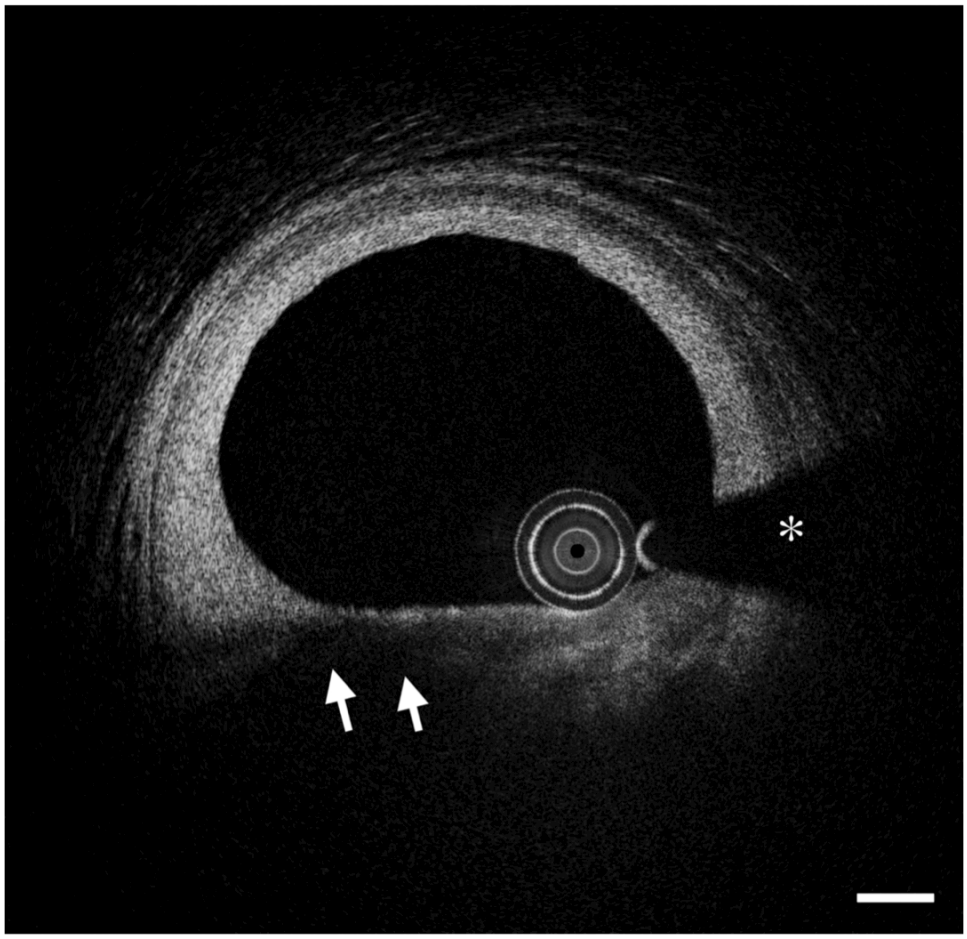

Online Figure 10. Tangential signal dropout. Arrows point to a region with low IVOCT signal intensity that is likely caused by attenuation of light as it propagates tangentially to the luminal surface. Scale bar represents 500 μm. IVOCT technology, image contributor and institution, and commercial IVOCT vendor for each Figure is provided in Online Appendix B. Abbreviations as in Online Figure 1.

Strut orientation artifact

Sometimes, when the catheter is near a stented artery wall, stent struts form a pinwheel pattern, appearing to face the catheter (Online Fig. 11). This artifact has also been termed as the "sunflower" artifact or the "merry-go-round" artifact due to its distinctive appearance.

Obliquity, eccentricity, and problems of vessel curvature

Similar to IVUS, when the catheter is not parallel to the longitudinal axis of the vessel wall or the optical beam is not at a 90° angle with respect to the artery wall, the image may undergo elliptical distortion, making measurements less accurate.

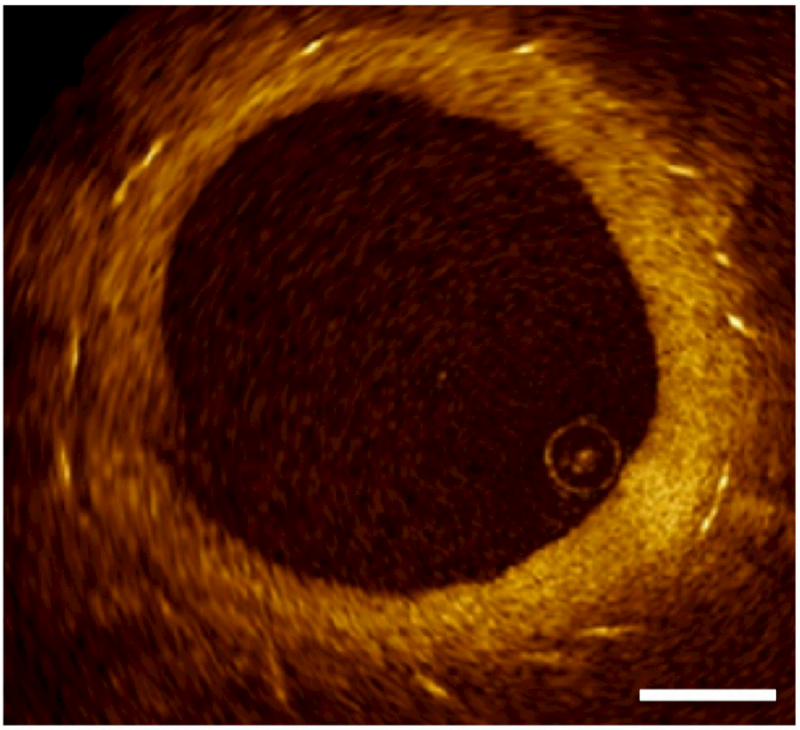

Online Figure 11. Strut orientation artifact. Stent struts appear to always face the catheter, an effect that is more pronounced when the catheter is located towards one side of the vessel. Scale bar represents 500 μm. IVOCT technology, image contributor and institution, and commercial IVOCT vendor for each Figure is provided in Online Appendix B. Abbreviations as in Online Figure 1.

Problem of spatial orientation

Also, like IVUS, there is no frame of reference for the spatial orientation (anterior, posterior, left, right) of IVOCT images. This lack of spatial orientation may make it difficult to register and compare other imaging modalities such as angiography to the IVOCT dataset. When present, landmarks such as side branches, presence of adventitial fat, visualization of the adjacent coronary vein, etc. may aid in determining the spatial orientation of IVOCT data and registering IVOCT with images from other imaging modalities.

4. IVOCT Image Display Techniques

Intensity scaling

Because the dynamic range of the IVOCT signal is often too large to be displayed by conventional display monitors, IVOCT image intensities are commonly shown as the logarithm of the IVOCT signal. A logarithmic scaling compresses the range of the data for display, bringing weaker features within the dynamic range of an observer at a computer screen. Alternatively, more general linear or nonlinear transformations (i.e. *gamma curves*) may be used to map the measured signal to displayed intensity. Caution should be applied when interpreting data using any scaling scheme other than

logarithmic, as most OCT analysis criteria have been developed and validated using a logarithmic scaling scheme.

Color mapping

The visualization of an IVOCT image requires a mapping of the OCT signal intensity to a color space that can be displayed on a monitor (Online Fig. 1). The simplest choice is grayscale (low is black, high is white) or inverted grayscale; this is also a safe option for colorblind users. A popular color map is the "sepia" scale, ranging from black (low OCT signal) through brown, gold, yellow and white (high OCT signal). The darkened environment of a catheterization laboratory favors light-on-dark color scales, but specific analysis, post-processing tasks, and user preferences may lead to different color mapping choices. Certain color mappings (e.g. rainbow-like) can bring out faint details in an image, but also strongly influence the shape-perception of the visualized data, and hence, measurements made in the image.

L-mode display

An L-mode view is a longitudinal section or longitudinal reconstruction of an IVOCT pullback dataset at a particular rotational angle. As with IVUS, the plane through which the longitudinal section is taken should intersect the center of mass of the artery or the lumen. Distance measurements can be made using the L-mode images when the frame rate and pullback speeds are known. Distance measurements in the longitudinal direction are more accurate when obtained through the center of the catheter. Care should be taken when interpreting L-mode images, as motion artifacts can cause the appearance of repeated structures, disappearance of structures that exist, or oscillation of the artery wall microstructure. L-mode image quality also depends on the frame-to-frame spacing, which affects the resolution of the L-mode imaging along the longitudinal dimension.

Three-dimensional visualization

3D visualization including cutaway or flythrough views of volume renderings have been utilized to display IVOCT datasets. These representations encompass multiple frames of a pullback, rather than showing only one cross-sectional image at a time. These methods of visualization may be advantageous as they can efficiently provide an overview of the artery wall anatomy. There are many different parameters such as pitch/frame-to-frame spacing, *segmentation*, *opacity tables*, *shading*, and color maps, which can affect how these visualization formats appear to the end user. At present, there are no standards for 3D visualization for IVOCT, and as a result, definitive artery wall diagnoses should only be made using cross-sectional IVOCT image data.

5. Image Acquisition Protocols

Image Acquisition Techniques

TD-OCT Image Acquisition Protocols

Proximal balloon occlusion technique: A 6 Fr or greater diameter guiding catheter can accommodate the TD-OCT imaging probe (ImageWire™, St. Jude Medical/LightLab Imaging, Westford, MA) and the proximal occlusion balloon system (Helios™, St. Jude Medical/LightLab Imaging, Westford, MA). Lactated Ringer's warmed to a temperature of

37° is the recommended flushing media since it causes less arrhythmia and myocardial ischemia compared to saline. The occlusion balloon catheter is advanced a few millimeters beyond the target site under the guidance of a 0.014" angioplasty wire. The guide wire is then removed and the IVOCT imaging probe is inserted through the central guide wire lumen (over-the-wire lumen) of the occlusion balloon. With the ImageWire™ held in place, the occlusion balloon is withdrawn until it is proximal to the target. To clear blood from the imaging site, the occlusion balloon is inflated at very low pressure (0.3-0.5 atm) by a dedicated inflation device. Lactated Ringer's solution is infused into the coronary artery from the distal tip of the occlusion balloon at a flow rate of 0.5-1.0 ml/s. Flush is administered typically via a power injector connected to the end-hole of the balloon occlusion catheter. Infusion should start a few seconds prior to balloon inflation to get clear images of the artery wall when the IVOCT image recording starts. The length of the target site is typically imaged with an automatic pullback device that translates at a rates ranging from 0.5-2.0 mm/sec. Images are typically acquired at a speed of 15.4 frames/sec. Imaging should be terminated earlier if any signs of patient intolerance, arrhythmia, or hemodynamic instability are encountered.

Non-occlusive flushing technique: A 6Fr or greater diameter guiding catheter is recommended for TD-OCT imaging with a non-occlusive flushing technique. Viscous iso-osmolar contrast media(109) or a mixture of low molecular weight dextrose and lactated Ringer's solution(110) has been successfully utilized for non-occlusive flushing. The IVOCT ImageWire™ can be advanced directly through the guiding catheter distal to the region of interest. As the IVOCT imaging wire can be difficult to maneuver, the ImageWire™ may alternatively be directed distally to the region of interest using a single lumen micro-catheter. Once the IVOCT ImageWire™ is positioned distally to the region of interest, and the guiding catheter is coaxially and deeply positioned within the coronary ostium, correct guide catheter position allowing for efficient blood clearing can be tested by manual injection of a small flush bolus through the guide catheter prior to imaging, if needed. Automated IVOCT pullback (pullback speed is typically between 2–4 mm/sec) is performed during either manual contrast injection through the guide catheter using a syringe or automatically using a power injector (typical flush rate 3.0 ml/s), connected to the standard Y-connector of the guiding catheter. A pullback duration limit (e.g. 30 s) may be set by default on the console, but imaging should be terminated earlier if any signs of patient intolerance, arrhythmia or hemodynamic instability are observed. After completion of pullback, flushing should be stopped immediately to limit the injected flush volume.

FD-OCT Image Acquisition Protocols

A 6Fr or larger diameter guiding catheter is recommended for FD-OCT imaging. Lactated Ringer's solution(54), viscous iso-osmolar contrast media(111), and mixtures of lactated Ringer's and contrast media or low molecular weight dextrose can be used for non-occlusive flushing, although higher viscosity solutions have been found to provide superior results. The IVOCT imaging catheter is advanced distally into the coronary artery via a standard angioplasty guide wire (0.014"). As with the non-occlusive TD-OCT technique, care should be taken to position the guide catheter coaxially and deeply into the coronary ostium. Correct guide catheter position can be confirmed by manual injection of a small flush bolus through the guide catheter prior to imaging, if needed. Automated IVOCT pullback is performed during either manual contrast injection through the guide catheter using a syringe or automatically using a power injector (typical flush rate 3.0 ml/s) connected to the standard Y-piece of the guiding catheter. Automated

IVOCT pullback speeds for FD-OCT systems typical ranges from 10–40 mm/sec. Flushing should be terminated when the region of interest has been imaged, blood re-enters the image, or the IVOCT catheter optics enter the guide catheter.

6. Qualitative Assessment

Dissections and Complications After Intervention

Dissections. Because of the similarity of IVOCT and IVUS appearance of dissections (Evidence Level: High), definitions are adopted from JACC IVUS Consensus Document. For completeness, these definitions are presented below:

"The classification of dissections into five categories is recommended:

Intimal: Limited to the intima or atheroma, and not extending to the media.

Medial: Extending into the media.

Adventitial: Extending through the EEM.

Intramural hematoma: An accumulation of [blood or] flushing media within the medial space, displacing the internal elastic membrane inward and EEM outward. Entry and/or exit points may or may not be observed.

Intra-stent: Separation of intima or neointimal hyperplasia from stent struts.

The severity of a dissection can be quantified according to: 1) depth into plaque; 2) circumferential extent (in degrees of arc) using a protractor centered on the lumen; 3) length using motorized transducer pullback; 4) size of residual lumen (CSA); and 5) CSA of the luminal dissection. Additional descriptors of a dissection may include the presence of a false lumen, the identification of mobile flap(s), the presence of calcium at the dissection border, and dissections in close proximity to stent edges."

Additionally, the severity of a dissection can be furthermore quantified by length of the mobile dissection flap. Because of the 10-μm resolution of IVOCT, small intimal dissections, also termed small intimal disruptions, are frequently seen by IVOCT. The clinical significance of these smaller intimal defects is not known.

Unusual Lesion Morphology (Aneurysms, Pseudoaneurysms, True vs. False Lumen)

IVOCT definitions for aneurysms, pseudoaneurysms, true vs. false lumen are adopted from JACC IVUS Consensus Document, with the caveat that these definitions only apply when the EEM can be identified (Evidence Level: Low). For completeness, these definitions are presented below, as they appear in the JACC IVUS Consensus Document:

"True aneurysm: A lesion that includes all layers of the vessel wall with an EEM and lumen area >50% larger than the proximal reference segment.

Pseudoaneurysm: Disruption of the EEM, usually observed after intervention.

True versus false lumen: A true lumen is surrounded by all three layers of the vessel-intima, media, and adventitia. Side branches communicate with the true, but not with the

false lumen. A false lumen is a channel, usually parallel to the true lumen, that does not communicate with the true lumen over a portion of its length."(112)

Special Considerations

Serial examination of atheroma progression/regression. Owing to its capability to characterize the microstructural detail of the coronary wall, IVOCT may be used to evaluate the progression/regression of specific atheroma features. Progression and regression can be considered an increase or decrease, respectively, in necrotic core and macrophages, and a decrease or increase, respectively in cap thickness, fibrous tissue or calcium (Evidence Level: Low). IVOCT cannot assess progression/regression of the atheroma thickness, area, or volume when the IEM or EEM cannot be identified. Progression/regression of such features has not been prospectively studied in large randomized trials.

Interventional target lesion assessment. Because the capability of IVOCT to interrogate the structure of the arterial wall is superior to angiography, this technology may be used to obtain additional information prior to angioplasty or stent implantation (Evidence Level: Low). However, the clinical significance of this additional information needs to be further established in randomized controlled trials.

Serial examination of stents. Longitudinal studies (pre/post-intervention vs. follow-up) can be used to evaluate the tissue coverage response of the artery to stent implantation (94,113,114). For these studies, stents are typically imaged at baseline using automated pullback at multiple time points. The IVOCT stent datasets are then registered using landmarks such as the stent edges and side branches. Following registration, the stents are compared using qualitative or quantitative measurements. At present the clinical significance of follow up stent findings of increased coverage or malapposition is not known. As with IVUS, IVOCT can be utilized to evaluate restenosis (as per JACC IVUS Consensus Document). It is important to note that in order to achieve optimal consistency across multiple serial examinations, care should be taken to use the same IVOCT system type (TD-OCT or FD-OCT), IVOCT catheter type, guide catheter diameter, and image acquisition method (i.e. occlusive or non-occlusive) and flush settings.

7. Quantitative Measurements

Border Identification

Lumen border. The vessel lumen can be traced at the boundary between the lumen and the leading edge of the intima using automatic, semiautomatic, or manual means. Care should be taken to avoid interpreting artifacts such as shadowing as being part of the artery lumen.

IEM border (intima-media border). For atheroma in which the IEM can be identified, it can be traced at the boundary between the intima and media using automatic, semiautomatic, or manual means. For atheroma in which the IEM cannot be identified due to the diminished penetration of the IVOCT light through the plaque, the IEM border cannot be delineated. It is therefore recommended that the intima-media border not be evaluated in these plaques.

EEM border (media-adventitia border). For plaques in which the EEM can be identified, it

can be traced at the boundary between the media and adventitia using automatic, semiautomatic, or manual means. For atheromas in which the EEM cannot be identified, due to the diminished penetration of the IVOCT light through the plaque, the EEM border cannot be delineated. It is therefore recommended that the media-adventitia border not be evaluated for these plaques.

Stent contour. The stent area can be delineated by tracing the contour of the stent. Investigators have used the leading edge of the stent strut surface reflection or the axial center of the stent to trace this contour. *Contour interpolation*, such as polynomial and spline interpolation of the lines between the strut anchors have been used.

Strut borders. Since light cannot penetrate metallic structures, the surfaces of struts are seen in IVOCT images with subsequent outer shadowing of the IVOCT signal in the image. When struts are present, artifacts frequently seen include saturation and blooming artifacts. When struts are covered by a significant amount of tissue, the surface reflection of the strut may not be identified and the presence of the strut can only be determined by visualization of the shadow deep to the strut. Furthermore, the strut reflection may not be parallel to the lumen surface but may be at an angle. Because of these issues, identification of the leading edge of the strut can sometimes be difficult. Preferred approaches for strut segmentation is a topic of future investigation and discussion.

Plaque and plaque component borders. Delineation of plaques and plaque components have been accomplished using qualitative IVOCT image interpretaion criteria and manual computer tracing. Due to the limited penetration depth of IVOCT for lipid-containing tissues, the deep border of plaques and lipid-containing regions cannot be clearly identified in many cases. The number of quadrants that a plaque subtends has been used to estimate the plaque size, but the relationships between this parameter and plaque thickness and area have not been determined.

Thrombus. Red or white thrombus borders may be delineated automatically, semiautomatically, or by manual tracing. Red thrombi attenuate light and as a result, it may be difficult to identify the deep border of red thrombi.

Macrophage accumulation borders. Macrophage accumulations can be traced using automatic, semiautomatic, or manual tracing means. Since the presence or absence of macrophage accumulations has only been evaluated in plaques, macrophage accumulations should not be traced in areas of normal artery wall, intimal hyperplasia, or side branches. Care should be taken so that features such as elastic laminae, cholesterol crystals, and saturation artifacts not be interpreted as macrophages.

Length and volume measurements

Length measurements can be obtained in IVOCT datasets that are acquired using automated pullback. The slice thickness (image spacing) in millimeters is the pullback rate (mm/s) times the frame rate (s). When the vessel is curved, it should be noted that length measurements are only accurate when accomplished in the center of the image displayed in Cartesian coordinates. Motion artifacts can decrease the accuracy of length measurements. Volume measurements can be made using *Simpson's rule* where the areas of each cross section in a pullback multiplied by the slice thickness (frame-frame spacing) are added over the segmented volume of interest.

8. IVOCT Validation

Ex vivo human tissue

IVOCT images acquired *ex vivo* appear similar to those acquired *in vivo*, even though postmortem changes may result in different arterial optical properties. The extent to which temperature, freezing, fixation, or time from excision/death affects the arterial optical tissue properties, and therefore the IVOCT signal, is not well understood. Until studies are conducted to demonstrate no changes, it is recommended that histopathologic correlation studies be on arterial tissue that is as fresh as possible and at physiological temperature (37° C). Most *ex vivo* studies have also been conducted while the tissue is at least partially in buffered saline to avoid morphological changes caused by osmotic flow. Accurate registration can be accomplished by applying fiducial ink marks on the specimen in a manner such that the ink marks can be visualized on both the OCT image and the corresponding histologic slide. When comparing OCT and histology measurements, OCT and histology images should be corrected for estimates of refractive index and tissue shrinkage, respectively.

Known challenges with histopathologic correlation studies include the lower penetration depth of IVOCT, especially through lipid-containing tissue, which may decrease accuracy of IVOCT for delineating some structures deep within the arterial wall. Mixed plaques may artificially diminish measured IVOCT accuracies when only one histopathologic diagnosis is rendered.

Animal models

Studies have described the utilization of IVOCT to investigate architectural arterial features in wild type and ApoE knockout mice(11,115). Studies in normal and cholesterol-fed balloon-injured New Zealand and Watanabe rabbit carotids, abdominal aortas, and iliac arteries have been used to confirm the ability of IVOCT to investigate stent healing, assess vessel morphology, and identify lipid-containing plaques *in vivo*(12,18,116,117). Imaging in swine *in vivo* enables the interrogation of a coronary tree that is very similar to that of humans. Recognized differences between normal swine and human coronary arteries include a greater susceptibility to motion artifact and absence of atherosclerosis for native swine. Swine models for atherosclerosis are also emerging that may be appropriate for IVOCT studies (118,119). Studies in both animal models have demonstrated very high correlation between IVOCT images of superficial arterial structures *in vivo* and histology. In swine, IVOCT has been shown to be able to correctly identify all of the vessel wall layers, dissections, thrombus, and stent tissue coverage when it is greater than axial resolution of the IVOCT system. Animal models may potentially be used to assess IVOCT's accuracy for quantifying plaque progression/regression longitudinally. Additional studies need to be conducted in order to validate the capability of IVOCT to monitor progression/regression.

Correlation with existing imaging modalities

Correlation between IVOCT images and other existing modalities is considered an important area of research for evaluating the potential role of IVOCT clinically. Since histopathology cannot be conducted reliably in human coronaries *in vivo*, IVOCT has also been utilized in some correlative imaging studies as a surrogate for histopathology *in vivo.* Typically, registration between IVOCT and other imaging modalities is accomplished using landmarks such as side branches and stent edges. Accurate registration between imaging modalities may be challenging, due to problems with

aligning image orientations and the dynamic nature of the coronary arteries *in vivo*. Furthermore, the depth and volume of IVOCT images are different from other imaging modalities, making it difficult to compare image features that rely on the identification of the IEM or EEM. When using IVOCT as a surrogate for histopathology, it is important to take into account the reported accuracies of IVOCT, to recognize that some histologic features have not been determined to be distinguished by IVOCT, and that there is not a one-to-one relationship between terminologies used by pathologists and IVOCT researchers.

Phantoms

A standardized phantom model for IVOCT calibration would serve to enhance the reproducibility and reliability of future findings. Analysis software could make use of well tested, standardized phantoms to minimize systematic errors and variability in measurements induced by different IVOCT systems and catheters. Research into developing phantoms with varying compositional and mechanical properties that mimic the normal and pathologic human arterial wall is ongoing.

9. Specialized OCT Techniques

Polarization-Sensitive OCT

Light has a property termed *polarization* that can be changed by interaction with many materials, including some kinds of biological tissues that are highly organized and oriented, such as collagen, muscle, or connective tissue. These types of tissues exhibit *birefringence*, which modifies the polarization state of light in a predictable way. A conventional OCT system is vulnerable to image artifacts due to this effect: as the signal will wax and wane as the polarization state of the signal light evolves into and out of alignment with the polarization state of the reference light. This polarization-fading artifact can be eliminated by use of methods developed for fiber-optic telecommunications. However, the polarization signal can also be measured to determine the birefringence of the tissue under examination. This measurement provides additional information about the composition of the artery wall. Birefringence measurement can be accomplished with a number of methods, collectively known as polarization-sensitive OCT (PS-OCT). These methods commonly involve making OCT measurements while probing the tissue with multiple polarization states.

Doppler-OCT

OCT is capable of detecting blood flow in a way closely analogous to Doppler ultrasound. When the OCT probe light is backscattered from moving blood cells, it acquires a frequency shift due to the well-known *Doppler Effect*. This Doppler shift can be detected as a modulation of the *phase* of the OCT signal. Therefore, in addition to the conventional OCT image, encoded in the amplitude of the signal, one can obtain a flow image by decoding the phase changes in the OCT signal. As with Doppler ultrasound, the signal phase encodes the *velocity* of the scatterers, but only that component of the velocity that is in the direction of the OCT beam. Therefore, absolute velocity can only be determined if the relative angle of the OCT beam to the velocity direction is known. Doppler OCT data are commonly displayed in false color (red to blue) overlaid on the conventional OCT image, in a manner similar to the conventional Color Doppler ultrasound display method.

10. Reporting of IVOCT Studies

Reporting of IVOCT studies is identical to the recommendations of the reporting of IVUS studies as per JACC IVUS Consensus Document and is presented (modified) from this reference for completeness.

"Recommended Format and Minimum Content of Coronary [IVOCT] Reports
A written report for the [IVOCT] examination should be generated. The report helps to communicate relevant information and becomes an important part of the patient's medical record where it may pertain to clinical, legal, or fiscal issues. Although the length and complexity of the report will vary greatly depending on the needs of different operators and institutions, the minimum content should include:

1) Appropriate patient demographic information and date—reference to the accompanying angiographic and/or interventional report;

2) The reason for the [IVOCT] procedure;

3) A brief description of the [IVOCT] procedure, including the equipment used, the flush media, route of administration (e.g. manual vs. power injector and flow volume, flow rate), guide catheter used and the level of anticoagulation achieved, and the coronary arteries imaged;

4) The basic findings of the [IVOCT] pullback, including any measurements that were performed such as minimum lumen diameter, minimum stent area, plaque burden (when the IEM or EEM can be measured), or minimum cap thickness;

5) Any notable morphological plaque features such as [necrotic core, OCT-TCFA], dissection, calcium, or thrombus;

6) Changes in therapy that resulted from the information provided by [IVOCT]; and

7) Any [IVOCT]-related complications and any consequent therapy.

A more complete report should also include the analysis of three cardinal image slices—a distal reference segment, a worst target site, and a proximal reference segment. Lumen areas should be reported. IEM/EEM areas, calculated plaque area, plaque burden, and area stenosis should be reported if the IEM/EEM is visible. If a stent is present, minimum stent area, and a description of strut apposition should be included."

Online Tables

Online Table 1

Feature	Evidence Level	Representative References
Normal vessel wall	High	(1-5)
Atheroma	High	(1-5)
Fibrous plaque	High	(5,6,26) (4,6-8,22,23,26,27)
Fibrocalcific plaque	High	(4-10,26)
Lipid pool*	High	(4-9,11,12)
Necrotic core	Low	(5,28,29) (29-39)
Fibrous cap	High	(13,14,40-42)
Fibroatheroma	High	(4-9,11,12) (5,28,29) (26,29-39)(43,44)
OCT thin-capped fibroatheroma (OCT-TCFA)	High	(29,30,32-35,38-41,43-45) (29,31-34,36,38,40,46-49) (32,34,50)
Macrophage accumulations	Medium	(15,51)
Intimal vasculature	Low	(52,53)
Cholesterol crystals	Low	(16,54)
Erosion	Low	(30)
Dissections	High	(55-59)
Ruptured Plaque	High	(32,46,50,60-63)
Ulceration	Medium	(64,65)
Thrombus	High	(18) (17,66-69) (17,66-71) (72)
Stent		
Prolapse	High	(73-75)
Apposition	High	(76-79) (75)
OCT Strut Coverage	High	(19,20,71,80-96)
Restenosis	High	(21,97)
Bioabsorbable stents/scaffolds	High	(98,99) (100) (101) (102)

Online Table 1. Levels of evidence for different IVOCT image features and associated representative references. RBC – red blood cell. *Note: a lipid pool is defined histologically as a necrotic core or a region within pathological intimal thickening that contains extracellular lipid or proteoglycans.

Online Table 2

Feature	Penetration Depth	Representative References
Whole blood	Low	(103-105)
Normal vessel wall	High	(5,106)
Fibrous plaque	High	(5-8,26)
Fibrocalcific plaque	High	(4-10,26)
Lipid pool*	Low	(4-9,11,12)
Necrotic core	Low	(5,28,29)
Macrophage accumulations	Low	(15,51)
Red thrombus (RBC-rich)	Low	(17)
White thrombus (platelet-rich)	High	(17)

Online Table 2. Relative IVOCT penetration depths for different tissue types. RBC – red blood cell. *Note: a lipid pool is defined histologically as a necrotic core or a region within pathological intimal thickening that contains extracellular lipid or proteoglycans.

Online References

1. Brezinski ME, Tearney GJ, Bouma BE, et al. Optical coherence tomography for optical biopsy. Properties and demonstration of vascular pathology. Circulation 1996;93:1206-13.
2. Brezinski ME, Tearney GJ, Bouma BE, et al. Imaging of coronary artery microstructure (in vitro) with optical coherence tomography. Am J Cardiol 1996;77:92-3.
3. Kume T, Akasaka T, Kawamoto T, et al. Assessment of coronary intima--media thickness by optical coherence tomography: comparison with intravascular ultrasound. Circ J 2005;69:903-7.
4. Rieber J, Meissner O, Babaryka G, et al. Diagnostic accuracy of optical coherence tomography and intravascular ultrasound for the detection and characterization of atherosclerotic plaque composition in ex-vivo coronary specimens: a comparison with histology. Coron Artery Dis 2006;17:425-30.
5. Yabushita H, Bouma BE, Houser SL, et al. Characterization of human atherosclerosis by optical coherence tomography. Circulation 2002;106:1640-5.
6. Meissner OA, Rieber J, Babaryka G, et al. Intravascular optical coherence tomography: comparison with histopathology in atherosclerotic peripheral artery specimens. J Vasc Interv Radiol 2006;17:343-9.
7. Kawasaki M, Bouma BE, Bressner J, et al. Diagnostic accuracy of optical coherence tomography and integrated backscatter intravascular ultrasound images for tissue characterization of human coronary plaques. J Am Coll Cardiol 2006;48:81-8.
8. Kume T, Akasaka T, Kawamoto T, et al. Assessment of coronary arterial plaque by optical coherence tomography. Am J Cardiol 2006;97:1172-5.
9. Xu C, Schmitt JM, Carlier SG, Virmani R. Characterization of atherosclerosis plaques by measuring both backscattering and attenuation coefficients in optical coherence tomography. J Biomed Opt 2008;13:034003.
10. Kume T, Okura H, Kawamoto T, et al. Assessment of the coronary calcification by optical coherence tomography. EuroIntervention : journal of EuroPCR in collaboration with the Working Group on Interventional Cardiology of the European Society of Cardiology 2011;6:768-72.
11. Cilingiroglu M, Oh JH, Sugunan B, et al. Detection of vulnerable plaque in a murine model of atherosclerosis with optical coherence tomography. Catheter Cardiovasc Interv 2006;67:915-23.
12. Zimarino M, Prati F, Stabile E, et al. Optical coherence tomography accurately identifies intermediate atherosclerotic lesions--an in vivo evaluation in the rabbit carotid artery. Atherosclerosis 2007;193:94-101.
13. van der Meer FJ, Faber DJ, Perree J, Pasterkamp G, Baraznji Sassoon D, van Leeuwen TG. Quantitative optical coherence tomography of arterial wall components. Lasers Med Sci 2005;20:45-51.
14. Kume T, Akasaka T, Kawamoto T, et al. Measurement of the thickness of the fibrous cap by optical coherence tomography. Am Heart J 2006;152:755 e1-4.
15. Tearney GJ, Yabushita H, Houser SL, et al. Quantification of macrophage content in atherosclerotic plaques by optical coherence tomography. Circulation 2003;107:113-9.
16. Prabhudesai V, Phelan C, Yang Y, Wang RK, Cowling MG. The potential role of optical coherence tomography in the evaluation of vulnerable carotid atheromatous plaques: a pilot study. Cardiovasc Intervent Radiol 2006;29:1039-45.

17. Kume T, Akasaka T, Kawamoto T, et al. Assessment of coronary arterial thrombus by optical coherence tomography. Am J Cardiol 2006;97:1713-7.
18. Meng L, Lv B, Zhang S, Yv B. In vivo optical coherence tomography of experimental thrombosis in a rabbit carotid model. Heart 2008;94:777-80.
19. Kume T, Akasaka T, Kawamoto T, et al. Visualization of neointima formation by optical coherence tomography. Int Heart J 2005;46:1133-6.
20. Murata A, Wallace-Bradley D, Tellez A, et al. Accuracy of optical coherence tomography in the evaluation of neointimal coverage after stent implantation. JACC Cardiovasc Imaging 2010;3:76-84.
21. Nagai H, Ishibashi-Ueda H, Fujii K. Histology of highly echolucent regions in optical coherence tomography images from two patients with sirolimus-eluting stent restenosis. Catheter Cardiovasc Interv 2009.
22. Nadkarni SK, Pierce MC, Park BH, et al. Measurement of collagen and smooth muscle cell content in atherosclerotic plaques using polarization-sensitive optical coherence tomography. J Am Coll Cardiol 2007;49:1474-81.
23. Giattina SD, Courtney BK, Herz PR, et al. Assessment of coronary plaque collagen with polarization sensitive optical coherence tomography (PS-OCT). Int J Cardiol 2006;107:400-9.
24. Donnelly P, Maurovich-Horvat P, Vorpahl M, et al. Multimodality imaging atlas of coronary atherosclerosis. JACC. Cardiovascular imaging 2010;3:876-80.
25. van Soest G, Goderie TP, Gonzalo N, et al. Imaging atherosclerotic plaque composition with intracoronary optical coherence tomography. Neth Heart J 2009;17:448-50.
26. Manfrini O, Mont E, Leone O, et al. Sources of error and interpretation of plaque morphology by optical coherence tomography. Am J Cardiol 2006;98:156-9.
27. Kuo WC, Chou NK, Chou C, et al. Polarization-sensitive optical coherence tomography for imaging human atherosclerosis. Appl Opt 2007;46:2520-7.
28. van Soest G, Goderie T, Regar E, et al. Atherosclerotic tissue characterization in vivo by optical coherence tomography attenuation imaging. J Biomed Opt 2010;15:011105.
29. Kume T, Okura H, Yamada R, et al. Frequency and spatial distribution of thin-cap fibroatheroma assessed by 3-vessel intravascular ultrasound and optical coherence tomography: an ex vivo validation and an initial in vivo feasibility study. Circ J 2009;73:1086-91.
30. Kubo T, Imanishi T, Takarada S, et al. Assessment of culprit lesion morphology in acute myocardial infarction: ability of optical coherence tomography compared with intravascular ultrasound and coronary angioscopy. J Am Coll Cardiol 2007;50:933-9.
31. Barlis P, Serruys PW, Gonzalo N, van der Giessen WJ, de Jaegere PJ, Regar E. Assessment of culprit and remote coronary narrowings using optical coherence tomography with long-term outcomes. Am J Cardiol 2008;102:391-5.
32. Tanaka A, Imanishi T, Kitabata H, et al. Distribution and frequency of thin-capped fibroatheromas and ruptured plaques in the entire culprit coronary artery in patients with acute coronary syndrome as determined by optical coherence tomography. Am J Cardiol 2008;102:975-9.
33. Akasaka T, Kubo T, Mizukoshi M, et al. Pathophysiology of acute coronary syndrome assessed by optical coherence tomography. J Cardiol 2010;56:8-14.
34. Kubo T, Imanishi T, Kashiwagi M, et al. Multiple coronary lesion instability in patients with acute myocardial infarction as determined by optical coherence tomography. Am J Cardiol 2010;105:318-22.

35. Regar E, van Soest G, Bruining N, et al. Optical coherence tomography in patients with acute coronary syndrome. EuroIntervention 2010;6 Suppl G:G154-60.
36. Jang IK, Tearney GJ, MacNeill B, et al. In vivo characterization of coronary atherosclerotic plaque by use of optical coherence tomography. Circulation 2005;111:1551-5.
37. Chen BX, Ma FY, Luo W, et al. [Characterization of atherosclerotic plaque in patients with unstable angina pectoris and stable angina pectoris by optical coherence tomography]. Zhonghua Xin Xue Guan Bing Za Zhi 2009;37:422-5.
38. Fujii K, Kawasaki D, Masutani M, et al. OCT assessment of thin-cap fibroatheroma distribution in native coronary arteries. JACC Cardiovasc Imaging 2010;3:168-75.
39. Raffel OC, Tearney GJ, Gauthier DD, Halpern EF, Bouma BE, Jang IK. Relationship between a systemic inflammatory marker, plaque inflammation, and plaque characteristics determined by intravascular optical coherence tomography. Arterioscler Thromb Vasc Biol 2007;27:1820-7.
40. Kashiwagi M, Tanaka A, Kitabata H, et al. Relationship between coronary arterial remodeling, fibrous cap thickness and high-sensitivity C-reactive protein levels in patients with acute coronary syndrome. Circ J 2009;73:1291-5.
41. Li QX, Fu QQ, Shi SW, et al. Relationship between plasma inflammatory markers and plaque fibrous cap thickness determined by intravascular optical coherence tomography. Heart 2010;96:196-201.
42. Kawasaki M, Hattori A, Ishihara Y, et al. Tissue characterization of coronary plaques and assessment of thickness of fibrous cap using integrated backscatter intravascular ultrasound. Comparison with histology and optical coherence tomography. Circulation journal : official journal of the Japanese Circulation Society 2010;74:2641-8.
43. Gonzalo N, Garcia-Garcia HM, Regar E, et al. In vivo assessment of high-risk coronary plaques at bifurcations with combined intravascular ultrasound and optical coherence tomography. JACC Cardiovasc Imaging 2009;2:473-82.
44. Raffel OC, Merchant FM, Tearney GJ, et al. In vivo association between positive coronary artery remodelling and coronary plaque characteristics assessed by intravascular optical coherence tomography. Eur Heart J 2008;29:1721-8.
45. Tanaka A, Imanishi T, Kitabata H, et al. Lipid-rich plaque and myocardial perfusion after successful stenting in patients with non-ST-segment elevation acute coronary syndrome: an optical coherence tomography study. Eur Heart J 2009;30:1348-55.
46. Raffel OC, Jang IK. Incidental finding of a ruptured thin-cap fibroatheroma by optical coherence tomography. Eur Heart J 2006;27:2393.
47. Fujii K, Masutani M, Okumura T, et al. Frequency and predictor of coronary thin-cap fibroatheroma in patients with acute myocardial infarction and stable angina pectoris a 3-vessel optical coherence tomography study. J Am Coll Cardiol 2008;52:787-8.
48. Chia S, Raffel OC, Takano M, Tearney GJ, Bouma BE, Jang IK. Comparison of coronary plaque characteristics between diabetic and non-diabetic subjects: An in vivo optical coherence tomography study. Diabetes Res Clin Pract 2008;81:155-60.
49. Chia S, Christopher Raffel O, Takano M, Tearney GJ, Bouma BE, Jang IK. In-vivo comparison of coronary plaque characteristics using optical coherence tomography in women vs. men with acute coronary syndrome. Coron Artery Dis 2007;18:423-7.

50. Tanaka A, Imanishi T, Kitabata H, et al. Morphology of exertion-triggered plaque rupture in patients with acute coronary syndrome: an optical coherence tomography study. Circulation 2008;118:2368-73.
51. MacNeill BD, Jang IK, Bouma BE, et al. Focal and multi-focal plaque macrophage distributions in patients with acute and stable presentations of coronary artery disease. J Am Coll Cardiol 2004;44:972-9.
52. Kitabata H, Tanaka A, Kubo T, et al. Relation of microchannel structure identified by optical coherence tomography to plaque vulnerability in patients with coronary artery disease. Am J Cardiol 2010;105:1673-8.
53. Takano M, Yamamoto M, Seino Y, Mizuno K. Neovascular microchannels in sirolimus-eluting stent occlusion at late phase. JACC. Cardiovascular interventions 2010;3:1202-3.
54. Tearney GJ, Waxman S, Shishkov M, et al. Three-dimensional coronary artery microscopy by intracoronary optical frequency domain imaging. JACC Cardiovasc Imaging 2008;1:752-61.
55. Adlam D, Ayers R, Channon KM. Intimal dissection causing late thrombosis of a covered stent: optical coherence tomography appearances. Circ Cardiovasc Interv 2009;2:359-60.
56. Gutierrez Garcia H, del Amo Hernandez E, Joseph Arnold R, San Roman JA. Coronary artery dissection assessed by optical coherence tomography. Rev Esp Cardiol 2009;62:587-8.
57. Ijsselmuiden A, Verheye S. Cocaine-induced coronary artery dissection. JACC Cardiovasc Interv 2009;2:1031.
58. Ishibashi K, Kitabata H, Akasaka T. Intracoronary optical coherence tomography assessment of spontaneous coronary artery dissection. Heart 2009;95:818.
59. Toutouzas K, Vaina S, Riga MI, Stefanadis C. Evaluation of dissection after coronary stent implantation by intravascular optical coherence tomography. Clin Cardiol 2009;32:E47-8.
60. Barlis P, Serruys PW, Devries A, Regar E. Optical coherence tomography assessment of vulnerable plaque rupture: predilection for the plaque 'shoulder'. Eur Heart J 2008;29:2023.
61. Kitabata H, Kubo T, Akasaka T. Identification of multiple plaque ruptures by optical coherence tomography in a patient with acute myocardial infarction: a three-vessel study. Heart 2008;94:544.
62. Chia S, Raffel OC, Takano M, Tearney GJ, Bouma BE, Jang IK. Association of statin therapy with reduced coronary plaque rupture: an optical coherence tomography study. Coron Artery Dis 2008;19:237-42.
63. Habara M, Terashima M, Suzuki T. Detection of atherosclerotic progression with rupture of degenerated in-stent intima five years after bare-metal stent implantation using optical coherence tomography. J Invasive Cardiol 2009;21:552-3.
64. Mizukoshi M, Imanishi T, Tanaka A, et al. Clinical classification and plaque morphology determined by optical coherence tomography in unstable angina pectoris. Am J Cardiol 2010;106:323-8.
65. Sawada T, Shite J, Shinke T, et al. Very late thrombosis of sirolimus-eluting stent due to late malapposition: Serial observations with optical coherence tomography. J Cardiol 2008;52:290-5.
66. Kim JS, Hong MK, Fan C, et al. Intracoronary thrombus formation after drug-eluting stents implantation: optical coherence tomographic study. Am Heart J 2010;159:278-83.

67. Shite J, Matsumoto D, Yokoyama M. Sirolimus-eluting stent fracture with thrombus, visualization by optical coherence tomography. Eur Heart J 2006;27:1389.
68. Takano M, Yamamoto M, Seino Y, Mizuno K. Thrombus in sirolimus-eluting stent identified by optical coherence tomography. Clin Cardiol 2010;33:E60.
69. Yamamoto M, Takano M, Murakami D, et al. Impact of small thrombus formation in restenotic bare-metal stent lesions associated with acute coronary syndrome: Identification by optical coherence tomography. Int J Cardiol 2010.
70. Capodanno D, Prati F, Pawlowsky T, et al. ClearWayRX system to reduce intracoronary thrombus in patients with acute coronary syndromes according to optical coherence tomography after abciximab intracoronary local infusion trial (COCTAIL): study rationale and design. J Cardiovasc Med (Hagerstown) 2010;11:130-6.
71. Itoh T, Fusazaki T, Kimura T, et al. "Intracoronary whirling current phenomenon" and thrombus formation after sirolimus-eluting stent implantation visualized by optical coherence tomography. Circ Cardiovasc Interv 2009;2:264-7.
72. Fujii K, Masutani M, Ohyanagi M. Contribution of organized thrombus to in-stent restenosis after sirolimus-eluting stent implantation: optical coherence tomography findings. Eur Heart J 2008;29:1385.
73. Jang IK, Tearney G, Bouma B. Visualization of tissue prolapse between coronary stent struts by optical coherence tomography: comparison with intravascular ultrasound. Circulation 2001;104:2754.
74. Luz A, Bisceglia T, Hughes C, Tammam K, Farah B, Fajadet J. Atherosclerotic plaque prolapse between coronary stent struts visualized by optical coherence tomography. Rev Port Cardiol 2010;29:143-6.
75. Bouma BE, Tearney GJ, Yabushita H, et al. Evaluation of intracoronary stenting by intravascular optical coherence tomography. Heart 2003;89:317-20.
76. Kim U, Kim JS, Lee JM, et al. The initial extent of malapposition in ST-elevation myocardial infarction treated with drug-eluting stent: the usefulness of optical coherence tomography. Yonsei Med J 2010;51:332-8.
77. Santos MC, Lin T, Barlis P. In-stent restenosis associated with stent malapposition: Seven year optical coherence tomography findings. Int J Cardiol 2010.
78. Sawada T, Shite J, Shinke T, et al. Persistent malapposition after implantation of sirolimus-eluting stent into intramural coronary hematoma: optical coherence tomography observations. Circ J 2006;70:1515-9.
79. Tanigawa J, Barlis P, Dimopoulos K, Di Mario C. Optical coherence tomography to assess malapposition in overlapping drug-eluting stents. EuroIntervention 2008;3:580-3.
80. Yao ZH, Matsubara T, Inada T, Suzuki Y, Suzuki T. Neointimal coverage of sirolimus-eluting stents 6 months and 12 months after implantation: evaluation by optical coherence tomography. Chin Med J (Engl) 2008;121:503-7.
81. Tian F, Chen YD, Sun ZJ, et al. Evaluation of neointimal coverage of overlapping sirolimus-eluting stents by optical coherence tomography. Chin Med J (Engl) 2009;122:670-4.
82. Takano M, Inami S, Jang IK, et al. Evaluation by optical coherence tomography of neointimal coverage of sirolimus-eluting stent three months after implantation. Am J Cardiol 2007;99:1033-8.
83. Nishiguchi T, Kitabata H, Tanaka A, et al. Very late stent thrombosis after drug-eluting stent in segment with neointimal tissue coverage. JACC Cardiovasc Imaging 2010;3:445-6.

84. Motreff P, Souteyrand G, Levesque S, et al. Comparative analysis of neointimal coverage with paclitaxel and zotarolimus drug-eluting stents, using optical coherence tomography 6 months after implantation. Arch Cardiovasc Dis 2009;102:617-24.
85. Moore P, Barlis P, Spiro J, et al. A randomized optical coherence tomography study of coronary stent strut coverage and luminal protrusion with rapamycin-eluting stents. JACC Cardiovasc Interv 2009;2:437-44.
86. Mills JS, N'Diaye C S, Yow E, et al. Preliminary observations using optical coherence tomography to assess neointimal coverage of a metal stent in a porcine model. Cardiovasc Revasc Med 2009;10:229-35.
87. Matsumoto D, Shite J, Shinke T, et al. Neointimal coverage of sirolimus-eluting stents at 6-month follow-up: evaluated by optical coherence tomography. Eur Heart J 2007;28:961-7.
88. Kim JS, Kim TH, Fan C, et al. Comparison of neointimal coverage of sirolimus-eluting stents and paclitaxel-eluting stents using optical coherence tomography at 9 months after implantation. Circ J 2010;74:320-6.
89. Kim JS, Jang IK, Fan C, et al. Evaluation in 3 months duration of neointimal coverage after zotarolimus-eluting stent implantation by optical coherence tomography: the ENDEAVOR OCT trial. JACC Cardiovasc Interv 2009;2:1240-7.
90. Kim JS, Fan C, Choi D, et al. Different patterns of neointimal coverage between acute coronary syndrome and stable angina after various types of drug-eluting stents implantation; 9-month follow-up optical coherence tomography study. Int J Cardiol 2009.
91. Ishigami K, Uemura S, Morikawa Y, et al. Long-term follow-up of neointimal coverage of sirolimus-eluting stents--evaluation with optical coherence tomography. Circ J 2009;73:2300-7.
92. Her AY, Lee BK, Shim JM, et al. Neointimal coverage on drug-eluting stent struts crossing side-branch vessels using optical coherence tomography. Am J Cardiol 2010;105:1565-9.
93. Guagliumi G, Sirbu V, Bezerra H, et al. Strut coverage and vessel wall response to zotarolimus-eluting and bare-metal stents implanted in patients with ST-segment elevation myocardial infarction: the OCTAMI (Optical Coherence Tomography in Acute Myocardial Infarction) Study. JACC Cardiovasc Interv 2010;3:680-7.
94. Gonzalo N, Barlis P, Serruys PW, et al. Incomplete stent apposition and delayed tissue coverage are more frequent in drug-eluting stents implanted during primary percutaneous coronary intervention for ST-segment elevation myocardial infarction than in drug-eluting stents implanted for stable/unstable angina: insights from optical coherence tomography. JACC Cardiovasc Interv 2009;2:445-52.
95. Davlouros PA, Nikokiris G, Karantalis V, et al. Neointimal coverage and stent strut apposition six months after implantation of a paclitaxel eluting stent in acute coronary syndromes: An optical coherence tomography study. Int J Cardiol 2010.
96. Chen BX, Ma FY, Luo W, et al. Neointimal coverage of bare-metal and sirolimus-eluting stents evaluated with optical coherence tomography. Heart 2008;94:566-70.
97. Gonzalo N, Serruys PW, Okamura T, et al. Optical coherence tomography patterns of stent restenosis. Am Heart J 2009;158:284-93.
98. Kozuki A, Shite J, Shinke T, et al. STELLIUM 1: First-in-man follow-up evaluation of bioabsorbable polymer-coated paclitaxel-eluting stent. Circ J 2010;74:2089-96.

99. Ormiston JA, Serruys PW, Regar E, et al. A bioabsorbable everolimus-eluting coronary stent system for patients with single de-novo coronary artery lesions (ABSORB): a prospective open-label trial. Lancet 2008;371:899-907.
100. Serruys PW, Onuma Y, Ormiston JA, et al. Evaluation of the second generation of a bioresorbable everolimus drug-eluting vascular scaffold for treatment of de novo coronary artery stenosis: six-month clinical and imaging outcomes. Circulation 2010;122:2301-12.
101. Serruys PW, Ormiston JA, Onuma Y, et al. A bioabsorbable everolimus-eluting coronary stent system (ABSORB): 2-year outcomes and results from multiple imaging methods. Lancet 2009;373:897-910.
102. Pinto Slottow TL, Pakala R, Waksman R. Serial imaging and histology illustrating the degradation of a bioabsorbable magnesium stent in a porcine coronary artery. Eur Heart J 2008;29:314.
103. Brezinski M, Saunders K, Jesser C, Li X, Fujimoto J. Index matching to improve optical coherence tomography imaging through blood. Circulation 2001;103:1999-2003.
104. Hoang KC, Edris A, Su J, et al. Use of an oxygen-carrying blood substitute to improve intravascular optical coherence tomography imaging. J Biomed Opt 2009;14:034028.
105. Villard JW, Feldman MD, Kim J, Milner TE, Freeman GL. Use of a blood substitute to determine instantaneous murine right ventricular thickening with optical coherence tomography. Circulation 2002;105:1843-9.
106. Jang IK, Bouma BE, Kang DH, et al. Visualization of coronary atherosclerotic plaques in patients using optical coherence tomography: comparison with intravascular ultrasound. J Am Coll Cardiol 2002;39:604-9.
107. Tearney GJ, Boppart SA, Bouma BE, et al. Scanning single-mode fiber optic catheter-endoscope for optical coherence tomography. Opt Lett 1996;21:543-5.
108. ten Hoff H, Korbijn A, Smith TH, Klinkhamer JF, Bom N. Imaging artifacts in mechanically driven ultrasound catheters. Int J Card Imaging 1989;4:195-9.
109. Prati F, Regar E, Mintz GS, et al. Expert review document on methodology, terminology, and clinical applications of optical coherence tomography: physical principles, methodology of image acquisition, and clinical application for assessment of coronary arteries and atherosclerosis. Eur Heart J 2010;31:401-15.
110. Kataiwa H, Tanaka A, Kitabata H, et al. Head to head comparison between the conventional balloon occlusion method and the non-occlusion method for optical coherence tomography. Int J Cardiol 2009.
111. Takarada S, Imanishi T, Liu Y, et al. Advantage of next-generation frequency-domain optical coherence tomography compared with conventional time-domain system in the assessment of coronary lesion. Catheter Cardiovasc Interv 2010;75:202-6.
112. Mintz GS, Nissen SE, Anderson WD, et al. American College of Cardiology Clinical Expert Consensus Document on Standards for Acquisition, Measurement and Reporting of Intravascular Ultrasound Studies (IVUS). A report of the American College of Cardiology Task Force on Clinical Expert Consensus Documents. J Am Coll Cardiol 2001;37:1478-92.
113. Katoh H, Shite J, Shinke T, et al. Delayed neointimalization on sirolimus-eluting stents: 6-month and 12-month follow up by optical coherence tomography. Circ J 2009;73:1033-7.

114. Chen BX, Ma FY, Luo W, et al. [Coronary artery atherosclerotic plaque and stent visualizations by optical coherence tomography]. Zhonghua Xin Xue Guan Bing Za Zhi 2006;34:130-3.
115. Muller G, Meissner S, Walther J, Cuevas M, Koch E, Morawietz H. Analysis of murine vascular function in vivo by optical coherence tomography in response to high-fat diet. Horm Metab Res 2009;41:537-41.
116. Prati F, Zimarino M, Stabile E, et al. Does optical coherence tomography identify arterial healing after stenting? An in vivo comparison with histology, in a rabbit carotid model. Heart 2008;94:217-21.
117. Fujimoto JG, Boppart SA, Tearney GJ, Bouma BE, Pitris C, Brezinski ME. High resolution in vivo intra-arterial imaging with optical coherence tomography. Heart 1999;82:128-33.
118. Granada JF, Kaluza GL, Wilensky RL, Biedermann BC, Schwartz RS, Falk E. Porcine models of coronary atherosclerosis and vulnerable plaque for imaging and interventional research. EuroIntervention 2009;5:140-8.
119. Tellez A, Krueger CG, Seifert P, et al. Coronary bare metal stent implantation in homozygous LDL receptor deficient swine induces a neointimal formation pattern similar to humans. Atherosclerosis 2010;213:518-24.

Appendix A: Technical Glossary

Absorption: A process whereby light energy is transferred to matter. Absorption can contribute to attenuation of the IVOCT light beam and the resultant IVOCT signal.

A-line: One line of an IVOCT image, representing the amount of reflected light or backscattering along the axial (depth) dimension.

A-line rate: The rate at which A-lines are acquired by the IVOCT system, usually specified in A-lines/second.

Attenuation: Loss of light due to scattering and/or absorption by flushing media, blood, or tissue, which results in a weaker IVOCT signal.

Axial dimension: The dimension of the IVOCT image that is collinear with the IVOCT catheter's light beam. Values along the axial dimension are equivalent to the data along the depth coordinates of the image.

Axial resolution: The minimum distance between two objects which can be resolved along the axial dimension.

Backscattered light or backscattering: The light that is reflected back (from tissue, blood, catheter sheath, guidewire, etc.) and collected by the IVOCT catheter. The IVOCT signal is proportional to the amount of backscattered light. Another term for backscattered light is **reflected light**.

Birefringence: A property of some tissues wherein refractive index (see below) differs for two orthogonal polarization states of light.

Cartesian coordinates: A rectangular coordinate system. IVOCT images are acquired in polar coordinates (see below) and then scan converted to be displayed in Cartesian coordinates.

Center of mass: The point (in Cartesian coordinates) that represents the location where the object is centered. May apply to intensity-weighted image or contour.

Circumferential or rotational dimension: The dimension of the IVOCT image that is perpendicular to the IVOCT catheter's light beam and in the direction tangential to catheter rotation.

Color Lookup Table (LUT): A table that matches the IVOCT image intensity value to a certain color that is displayed. A color LUT is also sometimes referred to as a **color map**.

Contour: The boundary of a certain object, such as lumen, stent, or plaque component.

Contour interpolation: Interpolation between points used to delineate a contour or boundary. The interpolation may be computed by fitting the points to **a polynomial**, **spline**, or other function.

Contrast: The difference in backscattered intensities that distinguish one object from other objects and the background.

Depth of focus: The axial distance over which the IVOCT intensity is collected from a spot that has a diameter that is ≤ $\sqrt{2}d_0$, where d_0 is the minimum spot diameter.

Detector: See **Photodetector**

DICOM: (Digital Imaging and Communication in Medicine) is a standard for exchanging medical images and other information, between medical imaging devices.

Doppler Effect: A change in frequency of radiation (i.e. light wavelength) that occurs when the radiation is scattered off of a moving object.

Drive Cable: A rotating cable that resides inside the catheter's sheath, runs the length of the catheter, and transmits torque from the proximal end to optical elements at the distal end of the catheter.

Dynamic range: The difference between minimum and maximum reflected signals that can be detected or visualized by the IVOCT system. A large dynamic range is a desired characteristic. The typical dynamic range of IVOCT images ranges from 30-50 *dB* (10^3 – 10^5).

Edge: The location in an image where there is a relatively large transition from one IVOCT signal to another. **Leading (trailing) edge** refer to the first (last) such edge in an object that is encountered along a vector that is pointing away from the catheter. **Lateral edge** refers to an edge that is along the lateral or transverse dimension of an object.

Gamma curves: Linear or nonlinear transformations that map the IVOCT signal to displayed intensity.

Helical scan: The typical scan pattern used to generate 3D IVOCT datasets, created by rapidly rotating catheter optics during slower translation along the catheter's long axis.

Focus or Focal Point: The point at which the IVOCT light emanating from the catheter converges to a spot with the smallest diameter.

Frame-to-frame spacing: The distance between adjacent image frames along the catheter's longitudinal dimension. The frame-to-frame spacing is also referred to as helical **Pitch**.

Frequency-Domain OCT (FD-OCT): A form of OCT that uses a light source that rapidly changes its wavelength as a function of time. Interference between the reference and sample arms is detected as a function of *optical frequency* (inversely proportional to the optical wavelength). Backscattering of light as a function of depth in tissue (A-lines) is computed from the wavelength-dependent interference using a Fourier Transform. Other terms for Frequency-Domain OCT include **Swept Source OCT (SS-OCT)** and **Optical Frequency Domain Imaging (OFDI**).

Fourier-Domain OCT: A class of OCT technologies that includes Frequency-Domain OCT (see above).

Gain: A multiplicative factor that can be used to adjust the IVOCT intensity values.

Interferometry: A technique whereby light from a sample is combined with light from a reference. Under conditions where the sample and reference arm path lengths match to within the coherence length of the light source, interference between the sample and reference arms may be detected. In OCT, analysis of the detected interference pattern provides information on the intensity of light that has been reflected from different depths within the artery wall.

Interference: Amplitude modulation observed when multiple coherent light waves are combined and detected.

Lateral or transverse resolution: The minimum distance between two resolvable objects along the circumferential dimension and in the plane of a single cross-sectional IVOCT image.

Longitudinal dimension: The dimension in an IVOCT 3D dataset that is parallel with the catheter's long axis and along the direction of pullback motion.

Longitudinal resolution: The minimum distance between two resolvable points along the longitudinal (pullback) dimension. This term is synonymous with **Pitch**. The Pitch determines the longitudinal resolution when the Pitch is larger than the spot diameter.

L-mode image: A longitudinal-mode represents an IVOCT image that has been generated by reconstructing a 3D IVOCT dataset along the longitudinal dimension at a particular rotational angle. L-mode images are also sometimes referred to as **longitudinal sections** or **longitudinal reconstructions.**

Near infrared (NIR) light: Light with wavelengths extending from 0.7 – 3 μm. IVOCT light is typically within the NIR range, centered around 1.3 μm.

Normalized Standard Deviation (NSD): A parameter that has been used for macrophage quantification. The NSD refers to the standard deviation of a region of interest, divided by the difference between the maximum and minimum IVOCT image values.

Opacity Tables: A table that is used to map IVOCT pixel values to various degrees of opacity or transparency, used in 3D volume rendering and visualization.

Optical Path Length: The physical length that light travels in a medium multiplied by the refractive index of the medium. For example, light traveling a physical distance of 2 mm in water (n = 1.33) will travel an optical path length of 2 x 1.33 = 2.66 mm.

PACS: (Picture Archive and Communication Systems) A computer system for storing, displaying, managing, and distributing medical images.

Penetration Depth: The depth within a tissue or object at which an IVOCT image signal has been attenuated (via scattering or absorption) to a level indistinguishable from the background noise.

Phase: A characteristic of a light wave that specifies the position of the wavefront at a given point in time and space. Phase changes may be used to estimate the motion of scatterers (flow) in tissue via the Doppler Effect. Relative phase changes between polarization states may be used to estimate tissue birefringence.

Photodetector: A semiconductor device that converts light into and electrical signal.

Polarization: A property of light described by the magnitude, orientation, and precession of its electric field. In a certain form of OCT, termed **Polarization-Sensitive OCT (PS-OCT)**, measurement of the polarization state of the light backscattered from within the tissue may be used to detect tissue birefringence and thus give additional compositional information.

Polar Coordinates: An r-θ coordinate system, where r is along the axial or depth dimension and θ is along the Circumferential dimension. IVOCT images with helical scan patterns are naturally acquired in Polar Coordinates but then are scan converted for display in Cartesian Coordinates.

Ranging depth or Scan Depth or Depth range: The total distance from the beginning to the end of an A-line.

Reference arm: The light path of an interferometer that provides the reference light..

Reflected light: The light that is returned from an object, which depends on refractive index mismatch and the shape of the interface between the object and the surrounding tissue or media. IVOCT measures reflected light that is collected by the catheter. Another term for reflected light is **backscattered light**.

Refractive index: A property of a material that governs the speed of light through the material.

Resolution: The minimum distance between closely spaced objects that can be independently distinguished by the imaging system.

Rotary Junction or Rotary Joint: A device that is configured to couple light from a non-rotating optical fiber (from the IVOCT system) into a rotating optical fiber that resides within the catheter. The Rotary Junction is frequently attached to a linear translation actuator that pulls or pushes the rotating optics of the catheter to create a helical scan of the vessel wall.

Sample arm: The light path of an interferometer that illuminates the sample (vessel tissue).

Saturation: A condition whereby the IVOCT signal strength exceeds an upper limit of the detector or detection electronics. This condition can result in a saturation or blooming artifact in the IVOCT image.

Scan Conversion: The process of converting an IVOCT image in polar coordinates to an IVOCT image in Cartesian coordinates.

Scattering: Redirection of of light by interaction with tissue. This process includes backscattering, which directs light back to the catheter where it can be collected to contribute to the IVOCT signal. Scattering in other directions causes attenuation or distortion of the IVOCT beam emanating from the catheter.

Segmentation: The process of delineating an object on an IVOCT image. Segmentation may be accomplished by drawing a contour around the object manually or by semi-automatic or automatic means.

Sensitivity: The minimum backscattered signal that is detectable by an OCT system.

Service-object pair (SOP): The fundamental functional element of a DICOM standard.

Single-mode optical fiber: A thin, flexible conduit or waveguide for the IVOCT light of well-defined optical path length that makes up the interferometer. It is also part of the catheter.

Shading: A change in the intensity of a volume rendering at a given location on the volume intended to provide depth perception, given certain illumination features, object and viewer perspectives, and simulated surface characteristics.

Shadow: Loss of IVOCT signal caused by something in the light path (e.g. stent struts, blood, macrophages, or other object) that attenuates the light deeper within the tissue.

Speckle: Grainy pattern that appears in IVOCT images due to interference of waves with random phase.

Spectral bandwidth: Total range of wavelengths produced by the IVOCT light source over an entire wavelength sweep. The axial resolution is inversely proportional to the spectral bandwidth.

Spot size: The diameter of the beam at any given axial or depth location.

Time-Domain OCT: A form of OCT that uses a broad bandwidth light source. Interference between the reference and sample arms is detected as a function of *time* as the optical path length of the reference arm is changed. The intensity of reflected light as a function of depth within tissue (A-lines) is derived from the envelope of the interference pattern.

Velocity of light: The speed at which light travels through a medium. The speed of light in air is $c_{air} = 3.0 \times 10^8$. The speed of light is lower in tissue $c_{tissue} = c_{air}/n_{tissue}$ where n_{tissue} is the refractive index, which ranges from approximately 1.33 – 1.5.

Volume Rendering: A three-dimensional representation of an IVOCT pullback dataset.

Z-offset: A difference in reference and sample arm path lengths that makes the scan converted IVOCT image appear to be expanded or contracted. Correction of the Z-offset is important for determining accurate dimensional measurements.

Appendix B: Figure Credits and Information

Print Figures

Figure 1. FD-OCT; Giulio Guagliumi, Bergamo; LightLab/St. Jude C7 system.

Figure 2A. FD-OCT; Guillermo Tearney, MGH and Giora Weisz, CUMC, MGH prototype system.

Figure 2B. FD-OCT; Guillermo Tearney, MGH and Evelyn Regar, ERMC; MGH prototype system.

Figure 2C. FD-OCT; Nieves Gonzalo Hospital Clinico San Carlos; LightLab/St. Jude C7 system.

Figure 2D. FD-OCT; Guillermo Tearney, MGH and Giora Weisz, CUMC; MGH prototype system.

Figure 3A. FD-OCT; Evelyn Regar, ERMC, Nieves Gonzalo, Hospital Clinico San Carlos ; LightLab/St. Jude C7 system.

Figure 3B. FD-OCT; Tom Adriaenssens, Leuven; LightLab/St. Jude C7 system.

Figure 3C.TD-OCT; Takashi Akasaka, Wakayama; LightLab/St. Jude M2 system.

Figure 3D. TD-OCT; Giulio Guagliumi, Bergamo; LightLab/St. Jude M2 system.

Figure 4. FD-OCT, Guillermo Tearney, MGH and Evelyn Regar, ERMC; MGH prototype system.

Figure 5A. TD-OCT; Takashi Akasaka, Wakayama; LightLab/St. Jude M2 system.

Figure 5B. FD-OCT; Guillermo Tearney, MGH and Sergio Waxman, Lahey Clinic; MGH prototype system.

Figure 6A. FD-OCT; Tom Adriaenssens, Leuven; LightLab/St. Jude C7 system.

Figure 6B. FD-OCT; Evelyn Regar, ERMC; Terumo prototype system.

Figure 7A. FD-OCT; Evelyn Regar, ERMC; LightLab/St. Jude C7 system.

Figure 7B. TD-OCT; Takashi Akasaka, Wakayama; LightLab/St. Jude, M2 system.

Figure 8A. FD-OCT; Guillermo Tearney, MGH and Evelyn Regar, ERMC; MGH prototype system.

Figure 8B. FD-OCT; Evelyn Regar, ERMC; Terumo prototype system.

Figure 8C. FD-OCT; Evelyn Regar, ERMC, Nieves Gonzalo, Hospital Clinico San Carlos; LightLab/St. Jude C7 system.

Figure 8D. FD-OCT; Evelyn Regar, ERMC; LightLab/St. Jude C7 system.

Figure 9A. FD-OCT; Evelyn Regar ERMC; LightLab/St. Jude C7 system.

Figure 9B. FD-OCT; Guillermo Tearney, MGH and Sergio Waxman, Lahey Clinic; MGH prototype system.

Figure 9C. TD-OCT; Giulio Guagliumi, Bergamo; LightLab/St. Jude M2 system.

Figure 9D. FD-OCT; Guillermo Tearney, MGH and Evelyn Regar, ERMC; MGH prototype system.

Online Figures

Online Figure 1. FD-OCT; Evelyn Regar, ERMC; LightLab/St. Jude C7 system.

Online Figure 2. FD-OCT; Nate Kemp, Volcano Corporation; Volcano Corporation prototype system.

Online Figure 3. FD-OCT; Tom Adriaenssens, Leuven; LightLab/St. Jude C7 system.

Online Figure 4. FD-OCT; Nate Kemp, Volcano Corporation; Volcano Corporation prototype system.

Online Figure 5. FD-OCT; Tom Adriaenssens, Leuven; LightLab/St. Jude C7 system.

Online Figure 6. FD-OCT; Guillermo Tearney, MGH and Evelyn Regar, ERMC, MGH prototype system.

Online Figure 7. FD-OCT; Tom Adriaenssens Leuven; LightLab/St. Jude C7 system.

Online Figure 8. Top row: FD-OCT; Evelyn Regar, ERMC, LightLab/St. Jude C7 system. Bottom row: FD-OCT; Guillermo Tearney, MGH and Sergio Waxman, Lahey Clinic, MGH prototype system.

Online Figure 9. FD-OCT; Guillermo Tearney, MGH and Sergio Waxman, Lahey Clinic, MGH prototype system.

Online Figure 10. FD-OCT; Guillermo Tearney, MGH and Evelyn Regar, ERMC, MGH prototype system.

Online Figure 11. TD-OCT; Marco Costa, Case Western, LightLab/St. Jude M2 system.

Appendix C: IWG-IVOCT Writing Committee Members and Affiliation

Adriaenssens, Tom MD - *Catholic University of Leuven, Leuven, Belgium*

Akasaka, Takashi MD - *Wakayama Medical University, Wakayama, Japan*

Barlis, Peter MD - *The University of Melbourne, Melbourne, Australia*

Bezerra, Hiram G. MD - *Case Western Reserve University, Cleveland, USA*

Bouma, Brett PhD - *Massachussets General Hospital, Boston, USA*

Bruining, Nico PhD - *Erasmus Medical Center, Rotterdam, The Netherlands*

Cho, Jin-man MD, PhD - *Kyung Hee University, Seoul, Korea*

Chowdhary, Saqib PhD - *University Hospital South Manchester, manchester, UK*

Costa, Marco A. MD, PhD, FACC - *Case Western Reserve University, Cleveland, USA*

de Silva, Ranil MD, PhD - *Royal Brompton Hospital, London, UK*

Dijkstra, Jouke PhD - *Leiden University Medical Center, Leiden, The Netherlands*

DiMario, Carlo MD, PhD - *Royal Brompton & Harefield Foundation NHS Trust, London, UK*

Dudek, Dariusz MD PhD- *Medical University of Warsaw, Warsaw, Poland*

Falk, Erling MD, PhD - *Aahrus University Hospital, Aahrus, Denemark*

Feldman, Marc D. MD - *University of Texas, Austin, USA*

Fitzgerald, Peter MD - *Stanford University, Stanford, USA*

Gonzalo, Nieves MD - *Hospital Clinico San Carlos, Madrid, Spain*

Granada, Juan F. MD - *Cardiovascular Research Foundation, NY, USA*

Guagliumi, Giulio MD - *Ospedali Riuniti, Bergamo, Italy*

Holm, Niels R. MD - *Aahrus University Hospital, Aahrus, Denemark*

Honda, Yasuhiro MD - *Stanford University, Stanford, USA*

Ikeno, Fumiaki MD - *Stanford University, Stanford, USA*

Kadota, Kazushige MD - *Karashiki Central Hospital, Okayama, Japan*

Kawasaki, Masanori MD - *Gifu University, Gifu, Japan*

Kochman, Janusz MD, PhD - *Medical University of Warsaw, Warsaw, Poland*

Koltowski, Lukasz MD - *Medical University of Warsaw, Warsaw, Poland*

Kubo, Takashi MD, PhD - *Wakayama Medical University, Wakayama, Japan*

Kume, Teruyoshi MD - *Stanford University, Stanford, USA*

Kyono, Hiroyuki MD - *University Hospitals at Case Western Reserve Medical, Cleveland, USA*

Lam, Cheung Chi Simon MD - *Queen Mary Hospital, Hong Kong*

Lamouche, Guy PhD - *The National Research Council Industrial Materials Institute, Quebec,Canada*

Lee, David P. MD - *Stanford University, Stanford, USA*

Leon, Martin B MD - *Columbia University Medical Center, NY, USA*

Maehara,, Akiko MD - *Cardiovascular Research Foundation, NY, USA*

Manfrini, Olivia MD - *University of Bologna,Bologna, Italy*

Mintz, Gary MD, FACC - *Cardiovascular Research Foundation, NY, USA*

Mizuno, Kyiouchi MD, PhD, FACC - *Nippon Medical School, Tokyo, Japan*

Morel, Marie-Ange MD - *Cardiolysis, Rotterdam, The Netherlands*

Nardkani, Seemantini PhD - *Massachussets General Hospital, Boston, USA*

Okura, Hiroyuki MD - *Kawasaki Medical School, Kawasaki, Japan*

Otake, Hiromasa MD, PhD - *Stanford University, Stanford, USA*

Pietrasik, Arkadiusz MD - *Medical University of Warsaw, Warsaw, Poland*

Prati, Francesco MD - *San Giovanni Hospital, Rome, Italy*

Räber, Lorenz MD - *University Hospital Bern, Bern, Switzerland*

Radu, Maria D. MD - *Rigshospital Copenhagen, Copenhagen, Denemark*

Regar, Evelyn MD, PhD - *Erasmus Medical Center, Rotterdam, The Netherlands*

Rieber, Johannes MD - *University of Munich, Munich, Germany*

Riga, Maria MD - *Athens University, Athens, Greece*

Rollins, Andrew PhD - *Case Western Reserve University, Cleveland, USA*

Rosenberg, Mireille PhD - *Massachussets General Hospital, Boston, USA*

Sirbu, Vasile MD - *Ospedali Riuniti, Bergamo, Italy*

Serruys, Patrick W.J.C. MD, PhD - *Erasmus Medical Center, Rotterdam, The Netherlands*

Shimada, Kenei MD - *Osaka Ekisaikai Hospital, Osaka, Japan*

Shinke, Toshiro MD - *Kobe University, Kobe, Japan*

Shite, Junya MD - *Kobe University, kobe, Japan*

Siegel, Eliot MD - *University of Maryland, Baltimore, USA*

Sonada, Shinjo MD - *University of Occupational and Enviormental Health, Fukuoka,Japan*

Suter, Melissa PhD - *Massachussets General Hospital, Boston, USA*

Takarada, Shigeho MD, PhD - *Wakayama Medical University, Japan*

Tanaka, Atsushi MD, PhD - *Massachussets General Hospital, Boston, USA, Wakayama Medical University, Japan*

Tearney, Guillermo J. MD, PhD, FACC - *Massachussets General Hospital, Boston, USA*

Terashima, Mitsuyasu MD, FACC - *Toyohashi Heart Center, Toyohashi, Japan*

Troels, Thim MD- *Aahrus University Hospital, Aahrus, Denemark*

Uemura, Shiro MD, PhD - *Nara Medical Center, Nara, Japan*

Ughi, Giovanni J. PhD - *Catholic University of Leuven, Leuven, Belgium*

van Beusekom, Heleen M.M. PhD - *Erasmus Medical Center, Rotterdam, The Netherlands*

van der Steen, Antonius F.W. PhD - *Erasmus Medical Center, Rotterdam, The Netherlands*

van Es, Gerrit-Ann PhD - *Cardiolysis, Rotterdam, The Netherlands*

van Soest, Gijs PhD - *Erasmus Medical Center, Rotterdam, The Netherlands*

Virmani, Renu MD - *CVPath, Gaithersburg, USA*

Waxman, Sergio MD - *Lahey Clinic, Burlington, USA*

Weissman, Neil J. MD - *Medstar, Washington, USA*

Weisz, Giora MD - *Columbia University Medical Center, NY, USA*

Appendix D: IWG-IVOCT Writing Committee Disclosure of Financial Interest

Writing Committee Members with no Financial Interest

Barlis, Peter MD
Bruining, Nico PhD
Cho, Jin-man MD, PhD
Dijkstra, Jouke PhD
DiMario, Carlo MD, PhD
Falk, Erling MD, PhD
Gonzalo, Nieves MD
Granada, Juan F. MD
Honda, Yasuhiro MD
Kawasaki, Masanori MD
Kume, Teruyoshi MD
Kyono, Hiroyuki MD
Lam, Cheung Chi Simon MD
Lamouche, Guy PhD
Lee, David P. MD
Manfrini, Olivia MD
Mizuno, Kyiouchi MD, PhD, FAAC
Morel, Marie-Ange MD
Nardkani, Seemantini PhD
Okura, Hiroyuki MD
Otake, Hiromasa MD, PhD
Pietrasik, Arkadiusz MD
Raber, Lorenz MD
Radu, Maria D. MD
Regar, Evelyn MD, PhD
Riga, Maria MD
Rosenberg, Mireille PhD
Serruys, Patrick W.J.C. MD, PhD
Shimada, Kenei MD
Siegel, Eliot MD
Sonada, Shinjo MD
Suter, Melissa PhD
Takarada, Shigeho MD, PhD
Tanaka, Atsushi MD, PhD
Terashima, Mitsuyasu MD, FACC
Uemura, Shiro MD, PhD
Ughi, Giovanni J. PhD
van Beusekom, Heleen M.M. PhD
van der Steen, Antonius F.W. PhD
van Es, Gerrit-Ann PhD
van Soest, Gijs PhD
Waxman, Sergio MD
Weissman, Neil J. MD
Weisz, Giora MD

Writing Committee Members with Disclosure of Financial Interest

Adriaenssens, Tom MD
Research Support and consulting fees from Abbott Vascular and St Jude Medical, IP in the field of image analysis
Akasaka, Takashi MD
Research or Grant support from Goodman, SJM Japan, Abbott Vascular Japan. Consulting fees/Honoraria from Goodman, SJM Japan, Terumo, GE Healthcare.
Bezerra, Hiram G. MD
Consulting fees from St Jude Medical
Bouma, Brett PhD
Research support from Terumo, MGH owned patents licensed to Terumo Corporation, rights to receive royalties from the MGH-Terumo licensing arrangement.
Chowdhary, Saqib PhD
Research Support and consulting fees from Biosensors and Boston Scientific
Costa, Marco A. MD, PhD, FACC
Consulting fees and honoraria from Medtronic, Scitech, Cordis, Abbott Vascular, and St. Jude. Speaker's Bureau fees from Daiichi Sankyo, Sano fi, and Eli Lilly
de Silva, Ranil MD, PhD
Research Support and consulting fees from A. Menarini Pharmaceuticals, Sanofi-Aventis, Servier Pharmaceuticals, and Medtronic UK.

Dudek, Dariusz MD
Research Grants or served as consultant/advisory board member for Abbott, Adamed, Biotronik, Balton, Bayer, Braun, BioMatrix, Boston Scientific, Boehringer Inc., Bristol Myers Squibb, Cordis, Cook, Eli Lilly, EuroCor, Glaxo, Invatec, Medtronic, Medicines
Feldman, Marc D. MD
Research support from Volcano
Fitzgerald, Peter MD
Consulting Fees/Honoraria from St. Jude Medical
Guagliumi, Giulio MD
Research Support and Consulting fees from Medtronic Vascular, Abbott,Boston Scientific, LightLab Imaging, Volcano Therapeutics, and Cordis
Holm, Niels R. MD
Research support from Boston Scientific
Ikeno, Fumiaki MD
Research Support and Consulting fees from Boston Scientific, Terumo Corporation, Volcano Therapeutics, and SVMI
Kochman, Janusz MD, PhD
Financial Benefit from Speaker's Bureau
Koltowski, Lukasz MD
Ownership / Founder of infrared group
Kubo, Takashi MD, PhD
Research grant support from Goodman Corporation, Cordis Corporation and Volcano Corporation
Leon, Martin B MD
Consulting fees from Abbott, Boston Scientific, Medtronic
Maehara, Akiko MD
Research Support from Boston Scientific Corporation and Volcano Corporation, Speaker Fee from Volcano Corporation
Mintz, Gary MD, FACC
Research Support and Consulting fees from Volcano, Boston Scientific (fellowship support), Volcano and Light Lab
Prati, Francesco MD
Research Support from Light Lab Inc.
Rieber, Johannes MD
Consulting Fees/Honoraria from St. Jude Medical
Rollins, Andrew PhD
Licensing and royalty income from LightLab Imaging and Carl Zeiss Meditec
Shinke, Toshiro MD
Consulting fees from Light Lab Inc.
Shite, Junya MD
Consultant fee: St Jude company, Goodman Company,
Sirbu, Vasile MD
Research Support from Light Lab Imaging.
Tearney, Guillermo J. MD, PhD, FAAC
Research support from Terumo, consulting fees from Merck and Samsung, MGH owned patents licensed to Terumo Corporation, rights to receive royalties from the MGH-Terumo licensing arrangement.
Virmani, Renu MD
Consulting fees / Honoraria from Abbott Vascular, Arsenal Medical, Atrium Medical Corporation, Biosensors International, Glaxosmithkline, Lutonix, Medtronic AVE, and WLGO